

THE ZEEMAN SPLITTING OF NUCLEAR QUADRUPOLE
RESONANCES IN SINGLE CRYSTALS OF ZINC BROMATE
HEXAHYDRATE AND COBALT BROMATE HEXAHYDRATE

b y

ALAN KENNETH GOODACRE
B.A., University of British Columbia, 1957

A THESIS SUBMITTED IN PARTIAL FULFILMENT OF
THE REQUIREMENTS FOR THE DEGREE OF

MASTER OF ARTS

in the Department
of

PHYSICS

We accept this thesis as conforming to the
required standard

THE UNIVERSITY OF BRITISH COLUMBIA

October, 1959.

A B S T R A C T

The Zeeman splitting of nuclear quadrupole resonances is discussed and a formula given for the split resonance frequencies as a function of the angle between the perturbing magnetic field and the symmetry axis of the crystalline electric field. The direction of this axis in the crystal can be found. If the electric field does not have cylindrical symmetry then for certain angles the spectrum becomes simplified and the directions of the three principal axes of the electric field gradient tensor can be found as well as the degree of asymmetry of the electric field.

These resonances are observed with the aid of a super-regenerative oscillator. A brief description of its operation is given as well as some signal to noise ratio considerations for various methods of detection of the resonances. The spectrometer used is described.

The Zeeman spectra of the nuclear quadrupole resonances of Br^{81} in single crystals of $\text{Zn}(\text{BrO}_3)_2 \cdot 6\text{H}_2\text{O}$ and $\text{Co}(\text{BrO}_3)_2 \cdot 6\text{H}_2\text{O}$ are observed. The accuracy of the observations is discussed and the conclusion is reached that within the error of the experiment the crystalline electric fields have cylindrical symmetry with four different directions of the symmetry axes in the crystal. They are parallel to the $\{1,1,1\}$ crystal axes. The crystals have cubic structure.

In presenting this thesis in partial fulfilment of the requirements for an advanced degree at the University of British Columbia, I agree that the Library shall make it freely available for reference and study. I further agree that permission for extensive copying of this thesis for scholarly purposes may be granted by the Head of my Department or by his representatives. It is understood that copying or publication of this thesis for financial gain shall not be allowed without my written permission.

Department of Physics

The University of British Columbia,
Vancouver 8, Canada.

Date October 1, 1959

TABLE OF CONTENTS

		<u>Page</u>
Chapter I	Zeeman Splitting of Nuclear Quadrupole Resonances.	1
Chapter II	The Super-regenerative Oscillator.	10
Chapter III	The Nuclear Quadrupole Resonance Spectrometer.	19
Chapter IV	Information Obtained about Single Crystals of $Zn(BrO_3)_2 \cdot 6H_2O$ and $Co(BrO_3)_2 \cdot 6H_2O$ from their Zeeman Spectra.	23
Bibliography		29

LIST OF ILLUSTRATIONS

<u>Figure</u>		<u>to follow page</u>
1	Plot of $\pm 3 \cos \Theta \pm (\cos^2 \Theta + 4 \sin^2 \Theta)^{\frac{1}{2}}$	6
2	Operation of Super-regenerative Oscillator with No Sample Present	
	a) Envelope of Rectified Oscillations. Coherent Operation.	
	b) Envelope of Rectified Oscillations. Incoherent Operation.	
	c) Rectified Output of Super-regenerative Oscillator. Coherent Operation.	
	d) Rectified Output of Super-regenerative Oscillator. Incoherent Operation.	12
3	Effect of Sample Upon Super-regenerative Oscillator Operation.	
	a) Envelope of Rectified Oscillations.	
	b) Rectified Output of Super-regenerative Oscillator.	13
4	Effect of the Quenching Process on the Signal to Noise Ratio of the Separate Detection Method.	16
5	Block Diagrams of the Apparatus	
	a) Separate Detection.	
	b) Phase-Sensitive Detection.	20
6	Wiring Diagrams	
	a) Crystal Controlled Oscillator and Tripler.	
	b) L - C Oscillator.	
	c) Mixer.	20

<u>Figure</u>		<u>to follow page</u>
7	Wiring Diagram. Frequency Modulated Quench Oscillator.	20
8	Field Strength vs. Distance Along Axis of One Helmholtz Coil.	22
9	A Crystal with Cubic Structure.	
	a) Crystal Faces.	
	b) Labelling of the z-symmetry Axes.	25
10	The Zeeman Splitting of the Nuclear Quadrupole Resonance of B_r^{81} in a Single Crystal of $Z_n(B_rO_3)_2 \cdot 6H_2O$. The $(1,1,1)$ Face is Perpendicular to the Axis of Rotation.	25
11	Zeeman Split Resonances of $Z_n(B_rO_3)_2 \cdot 6H_2O$. Crystal Mounted with the $(1,1,1)$ Face Perpendicular to the Axis of Rotation.	
	a) Self Detection with Phase Sensitive Detection.	
	b) Separate Detection with Phase Sensitive Detection.	
	c) Separate Detection. Rectified Noise.	26
12	Zeeman Split Resonances of $Co(B_rO_3)_2 \cdot 6H_2O$. Separate Detection. Rectified Noise	
	a) Coincidence of an Inner and Outer Line. Crystal Mounted with the $(1,1,1)$ Face Perpendicular to the Axis of Rotation.	
	b) Coincidence of Four Inner and Four Outer Lines. Crystal Mounted with the $(1,1,1)$ and $(1,1,\bar{1})$ Faces Parallel to the Axis of Rotation.	27

LIST OF PLATES

<u>Plate</u>		<u>to follow page</u>
I	The Spectrometer	22
II	Helmholtz Coils. Crystal Holder.	22

LIST OF TABLES

<u>Table</u>		<u>to follow page</u>
1	Observations of the Zeeman Spectra of $Zn(BrO_3)_2 \cdot 6H_2O$ and Calculations of the Crystal Field Parameters.	26
2	Observations of the Zeeman Spectra of $Zn(BrO_3)_2 \cdot 6H_2O$ and Calculations of the Crystal Field Parameters.	26
3	Observations of the Zeeman Spectra of $Co(BrO_3)_2 \cdot 6H_2O$ and Calculations of the Crystal Field Parameters.	27
4	Observations of Second Order Effects of the Zeeman Splitting of the Nuclear Quadrupole Resonance of $Co(BrO_3)_2 \cdot 6H_2O$.	27

A C K N O W L E D G E M E N T

I would especially like to thank Dr. J.M. Daniels for suggesting the topic of this thesis and his subsequent interest and guidance in all phases of the work. Also I appreciate the added discussions with Professor R.E. Burgess about the thesis. Mr. H.M. Zerbst has given me valuable assistance by designing and building the Helmholtz coils and crystal holder.

CHAPTER 1.ZEEMAN SPLITTING OF NUCLEAR QUADRUPOLE RESONANCES

Nuclear quadrupole resonances may be observed in a system where there exists a nucleus possessing an electric quadrupole moment located in an electric field which possesses a constant average electric field gradient. The resulting interaction energy depends on the orientation of the nucleus in the electric field. Transitions between adjacent energy levels may be induced by a radio frequency field which interacts with the nuclear magnetic dipole moment.

The nuclear charge distribution has rotational symmetry. Also, the electric fields found in crystals, where the requirement of a constant average electric field gradient may be met, often have cylindrical symmetry to a first approximation. The effect of higher order derivatives of the electric field on the interaction energy is too small to be observed.

The observable interaction energy of the system is:

$$U^E = ql^2 \left[\frac{3}{2} \cos^2 \Theta - \frac{1}{2} \right] V_{zz} \quad (1) \quad \text{where}$$

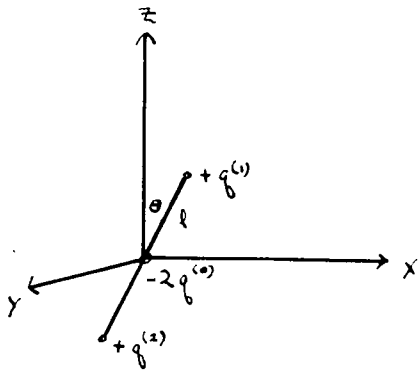
ql^2 is the quadrupole moment

Θ is the angle between the quadrupole symmetry axis and the electric field symmetry axis and

V_{zz} is defined by equation (8)

For example, consider the energy of orientation of a linear electric quadrupole where V_{zz} constant. If the four charges are initially at the origin and then moved to the position shown in the diagram

2.



(the quadrupole is in the
x-z plane and the super-
scripts refer to position.)

$-2q$ at $(0,0,0)$; $+q$ at $\pm(l \sin \theta, 0, l \cos \theta)$

the energy needed to do this is

$$U^E = q(V'^{(2)} - V'^{(0)}) + q(V'^{(1)} - V'^{(0)}) \quad (2)$$

but

$$\begin{aligned} (V'^{(2)} - V'^{(0)}) &= - \left(\frac{\partial V'}{\partial z} \right)_{z=0} l \cos \theta - \left(\frac{\partial V'}{\partial x} \right)_{x=0} l \sin \theta \\ &+ \frac{1}{2} \left(\frac{\partial^2 V'}{\partial z^2} \right)_{z=0} l^2 \cos^2 \theta + \frac{1}{2} \left(\frac{\partial^2 V'}{\partial x^2} \right)_{x=0} l^2 \sin^2 \theta \\ &+ \left(\frac{\partial^2 V'}{\partial x \partial z} \right)_{x=z=0} l^2 \cos \theta \sin \theta \end{aligned}$$

and

$$\begin{aligned} (V'^{(1)} - V'^{(0)}) &= + \left(\frac{\partial V'}{\partial z} \right)_{z=0} l \cos \theta + \left(\frac{\partial V'}{\partial x} \right)_{x=0} l \sin \theta \\ &+ \frac{1}{2} \left(\frac{\partial^2 V'}{\partial z^2} \right)_{z=0} l^2 \cos^2 \theta + \frac{1}{2} \left(\frac{\partial^2 V'}{\partial x^2} \right)_{x=0} l^2 \sin^2 \theta \\ &+ \left(\frac{\partial^2 V'}{\partial x \partial z} \right)_{x=z=0} l^2 \cos \theta \sin \theta \end{aligned}$$

therefore

$$\begin{aligned} U^E &= ql^2 \left(\frac{\partial^2 V'}{\partial z^2} \right)_{z=0} \cos^2 \theta + ql^2 \left(\frac{\partial^2 V'}{\partial x^2} \right)_{x=0} \sin^2 \theta \\ &+ 2ql^2 \left(\frac{\partial^2 V'}{\partial x \partial z} \right)_{x=z=0} \cos \theta \sin \theta \quad (3) \end{aligned}$$

If the z-axis is a symmetry axis then

$$\left(\frac{\partial^2 V'}{\partial x \partial z} \right)_{x=z=0} = 0 \quad (4a)$$

and

$$\left(\frac{\partial^2 V'}{\partial x^2} \right)_{x=0} = \left(\frac{\partial^2 V'}{\partial y^2} \right)_{y=0} \quad (4b)$$

gravity of the energy levels which cannot be observed in these experiments and will be neglected. Hence the usual formulation of the interaction energy is

$$U^E = qI^2 \left[\frac{3}{2} \cos^2 \Theta - \frac{1}{2} \right] V_{zz} \quad (1)$$

The quantum mechanical energy levels of the system may be found by replacing

$$\cos \Theta \quad \text{by} \quad \frac{m_z}{\sqrt{I(I+1)}} \quad (\text{where } I \text{ is the spin of the nucleus})$$

and

$$qI^2 \quad \text{by} \quad \frac{1}{4} qQ \quad \text{since the usual definition of the quadrupole moment is}$$

$$qQ \equiv \int_V \rho (3z^2 - r^2) d\tau \quad \text{where}$$

ρ is the nuclear charge density

r is the distance of the volume element $d\tau$ from the center of the nucleus

z is the projection of r on the axis of symmetry of the nucleus.

Also it is customary to use the projection of the quadrupole moment on the axis of quantization when this projection is a maximum. So we replace

$$Q \quad \text{by} \quad Q_I \frac{2(I+1)}{(2I-1)}$$

The energy levels are given by

$$U_{m_z}^E = qQ_I \frac{(3m_z^2 - I(I+1))}{4I(2I-1)} \quad (10)$$

where the symmetry axis of the electric field is the axis of quantization.

Zeeman splitting of the energy levels occurs when a homogenous magnetic field H is applied to the system. For our purposes the interaction energy between the nuclear magnetic dipole moment μ and the magnetic field will be

For convenience we set

$$\left(\frac{\partial^2 V'}{\partial x^2}\right)_{x=0} = V'_{xx} \quad ; \quad \left(\frac{\partial^2 V'}{\partial y^2}\right)_{y=0} = V'_{yy} \quad ; \quad \left(\frac{\partial^2 V'}{\partial z^2}\right)_{z=0} = V'_{zz}$$

so using equation 4a

$$U^E = qf^2 V'_{zz} \cos^2 \theta + qf^2 V'_{xx} \sin^2 \theta \quad (5)$$

It is mathematically convenient to use a potential V for the interaction energy such that

$$V_{xx} + V_{yy} + V_{zz} = 0 \quad (6)$$

Now there is an electron charge density at the nucleus so we have

$$V'_{xx} + V'_{yy} + V'_{zz} = V''_{xx} + V''_{yy} + V''_{zz} \quad (7)$$

where V'' is a new potential representing a spherically symmetric field. That is

$$V''_{xx} = V''_{yy} = V''_{zz}$$

We can rewrite equation 7 as

$$V'_{xx} - V''_{xx} + V'_{yy} - V''_{yy} + V'_{zz} - V''_{zz} = 0$$

or

$$V_{xx} + V_{yy} + V_{zz} = 0$$

where

$$V_{xx} = V'_{xx} - V''_{xx} \quad \text{etc.} \quad (8)$$

Using equations (4b), (5), (6), and (8) we find

$$U^E = qf^2 \left(\frac{3}{2} \cos^2 \theta - \frac{1}{2} \right) V_{zz} + qf^2 V''_{zz} \quad (9)$$

In nuclear quadrupole resonance experiments we are interested in differences between energy levels. The first term in equation (9) will give a set of energy levels whose "center of gravity" is constant, i.e. the arithmetical sum of the energy levels is zero. The second term represents a shift of the center of

much smaller than the unperturbed interaction energy. In this case the perturbing energy $U_{m_z}^M$ is

$$U_{m_z}^M = m_z \frac{\mu H}{I} \cos \Theta \quad (11)$$

where Θ is the angle between the applied magnetic field and the nuclear magnetic dipole moment. The energy levels of the system are given by

$$\begin{aligned} U_{m_z} &= U_{m_z}^E + U_{m_z}^M \\ &= A(3m_z^2 - I(I+1)) + 2m_z \xi \cos \Theta \quad (12) \end{aligned}$$

where

$$A = \frac{q Q_I V_{zz}}{4I(2I-1)}, \quad \xi = \frac{\mu H}{2I} = \frac{\gamma \hbar H}{2}$$

In this experiment $I = \frac{3}{2}$ and, in fact, the magnetic interaction energy in the state $m_z = \frac{1}{2}$ is too large to be considered as a perturbation of the electric interaction energy. The Hamiltonian for the case $I = \frac{3}{2}$ is, in general ¹

$$\begin{pmatrix} 3A + 3\xi \cos \Theta & \sqrt{3} \xi \sin \Theta e^{i\phi} & \sqrt{3} A \eta & 0 \\ \sqrt{3} \xi \sin \Theta e^{-i\phi} & -3A + \xi \cos \Theta & 2\xi \sin \Theta e^{i\phi} & \sqrt{3} A \eta \\ \sqrt{3} A \eta & 2\xi \sin \Theta e^{-i\phi} & -3A - \xi \cos \Theta & \sqrt{3} \xi \sin \Theta e^{i\phi} \\ 0 & \sqrt{3} A \eta & \sqrt{3} \xi \sin \Theta e^{-i\phi} & +3A - 3\xi \cos \Theta \end{pmatrix} \quad (13)$$

where Θ and ϕ are the polar angles of the magnetic field with respect to the axis of quantization and if

$$|V_{xx}| \leq |V_{yy}| \leq |V_{zz}| \quad \text{then the asymmetry}$$

parameter η is defined as

$$\eta = \frac{V_{xx} - V_{yy}}{V_{zz}} \quad (14)$$

For $\eta = 0$ and $\xi \ll A$ the only important off diagonal matrix elements are those connecting the $m_z = \pm \frac{1}{2}$ states and the Hamiltonian is

$$\begin{pmatrix} 3A + 3\xi \cos \Theta & 0 & 0 & 0 \\ 0 & -3A + \xi \cos \Theta & 2\xi \sin \Theta e^{i\phi} & 0 \\ 0 & 2\xi \sin \Theta e^{-i\phi} & -3A - \xi \cos \Theta & 0 \\ 0 & 0 & 0 & +3A - 3\xi \cos \Theta \end{pmatrix}$$

The roots of the secular equation are

$$\begin{aligned}\Lambda_1 &= 3A + 3\xi \cos \Theta \\ \Lambda_2 &= -3A + \xi (\cos^2 \Theta + 4 \sin^2 \Theta)^{\frac{1}{2}} \\ \Lambda_3 &= -3A - \xi (\cos^2 \Theta + 4 \sin^2 \Theta)^{\frac{1}{2}} \\ \Lambda_4 &= 3A - 3\xi \cos \Theta\end{aligned}$$

and for the allowed $\Delta m_2 = \pm 1$ transitions five resonances are expected but that with frequency of the order of $\frac{\xi}{h}$ will not be considered. The four resonance frequencies are given by (Figure 1)

$$h\omega = 6A \pm 3\xi \cos \Theta \pm \xi (\cos^2 \Theta + 4 \sin^2 \Theta)^{\frac{1}{2}} \quad (15)$$

The curves of the Zeeman split resonances are symmetrical about the unsplit frequency $6A$. The two resonances with the smaller frequency splitting are called the "inner lines" and the other two resonances are called the "outer lines".

In general the secular equation for the energy eigenvalues is

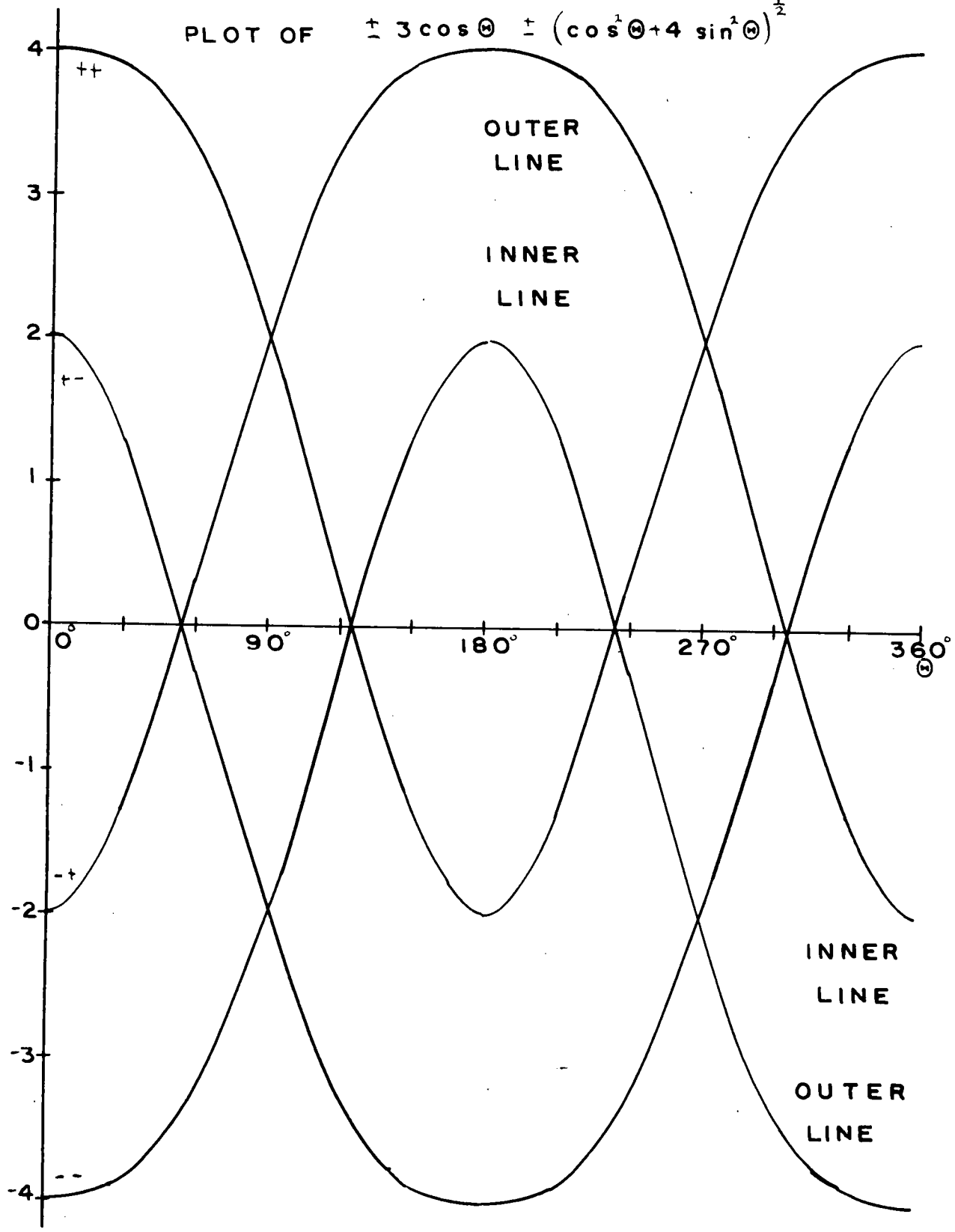
$$\begin{aligned}\Lambda^4 &- \Lambda^2 \{ 10\xi^2 + 18A^2 + 6A^2\eta^2 \} \\ &+ \Lambda \{ -48A\xi^2 + 72A\xi^2 \sin^2 \Theta - 24A\eta\xi^2 \sin^2 \Theta \cos 2\phi \} \\ &+ 81A^4 + 9A^4\eta^4 + 54A^4\eta^2 - 90A^2\xi^2 + 108A^2\xi^2 \sin^2 \Theta \\ &+ 9\xi^4 + 18A^2\eta^2\xi^2 - 36A^2\eta^2\xi^2 \sin^2 \Theta \\ &+ 72\xi^2 A^2 \eta \sin^2 \Theta \cos 2\phi \\ &= 0\end{aligned} \quad (16)$$

A simplification to a quadratic in Λ^2 occurs if the coefficient of Λ is made zero. This corresponds to two resonance frequencies being the same, or that

FIGURE 1

to follow page 6

PLOT OF $\pm 3 \cos \theta \pm (\cos^2 \theta + 4 \sin^2 \theta)^{\frac{1}{2}}$



the inner and outer lines coincide. This coefficient is zero when

$$\eta \cos 2\phi = 3 - \frac{2}{\sin^2 \ominus} \quad (17a)$$

If $\eta = 0$ the inner and outer lines will coincide when

$$\sin^2 \ominus = \frac{2}{3} \quad (17b)$$

then the roots of the secular equation are given by

$$\Lambda^2 = 5\xi^2 + 9A^2 \pm \sqrt{16\xi^4 + 108A^2\xi^2}$$

If $\xi \ll A$ and using the expansion $(1+x)^{\frac{1}{2}} = 1 + \frac{x}{2}$ for small x then

the four roots are

$$\begin{aligned} \Lambda_1 &= 3A + \sqrt{3}\xi + \frac{\xi^2}{3A} \\ \Lambda_2 &= -3A + \sqrt{3}\xi + \frac{\xi^2}{3A} \\ \Lambda_3 &= -3A - \sqrt{3}\xi - \frac{\xi^2}{3A} \\ \Lambda_4 &= 3A - \sqrt{3}\xi - \frac{\xi^2}{3A} \end{aligned}$$

and the three resulting resonance frequencies are given by

$$h\nu = 6A + \frac{2}{3}\frac{\xi^2}{A} \quad (18)$$

$$h\nu = 6A \pm 2\sqrt{3}\xi + \frac{2}{3}\frac{\xi^2}{A}$$

If $\eta \neq 0$ the inner and outer lines will coincide if

$$\eta \cos 2\phi = 3 - \frac{2}{\sin^2 \ominus} \quad (17b)$$

The directions of the three principal axes of the tensor describing the electric field gradient may be found by first examining the splitting of the inner lines to find the direction of the z-axis.

When the magnetic field is along the z-axis the Hamiltonian becomes

$$\begin{pmatrix} 3A + 3\xi & , & \sqrt{3}A\eta & , & 0 & , & 0 \\ \sqrt{3}A\eta & , & -3A - \xi & , & 0 & , & 0 \\ 0 & , & 0 & , & -3A + \xi & , & \sqrt{3}A\eta \\ 0 & , & 0 & , & \sqrt{3}A\eta & , & 3A - 3\xi \end{pmatrix}$$

and the roots of the secular equation are given by

$$\Lambda = +\xi \pm \sqrt{4\xi^2 + 12A\xi + 9A^2 + 3A^2\eta^2}$$

and

$$\lambda = -\xi \pm \sqrt{4\xi^2 - 12A\xi + 9A^2 + 3A^2\eta^2}$$

Using the expansion $(1+x)^{1/2} = 1 + \frac{x}{2} - \frac{x^2}{8}$ for small x the energy levels

are

$$\lambda_1 = 3A\left(1 + \frac{\eta^2}{3}\right)^{1/2} + \frac{2\xi}{\left(1 + \frac{\eta^2}{3}\right)^{1/2}} + \xi + \frac{2\xi^2}{3A\left(1 + \frac{\eta^2}{3}\right)^{3/2}} \frac{\eta^2}{3}$$

$$\lambda_2 = -3A\left(1 + \frac{\eta^2}{3}\right)^{1/2} + \frac{2\xi}{\left(1 + \frac{\eta^2}{3}\right)^{1/2}} - \xi - \frac{2\xi^2}{3A\left(1 + \frac{\eta^2}{3}\right)^{3/2}} \frac{\eta^2}{3}$$

$$\lambda_3 = -3A\left(1 + \frac{\eta^2}{3}\right)^{1/2} - \frac{2\xi}{\left(1 + \frac{\eta^2}{3}\right)^{1/2}} + \xi - \frac{2\xi^2}{3A\left(1 + \frac{\eta^2}{3}\right)^{3/2}} \frac{\eta^2}{3}$$

$$\lambda_4 = 3A\left(1 + \frac{\eta^2}{3}\right)^{1/2} - \frac{2\xi}{\left(1 + \frac{\eta^2}{3}\right)^{1/2}} - \xi + \frac{2\xi^2}{3A\left(1 + \frac{\eta^2}{3}\right)^{3/2}} \frac{\eta^2}{3}$$

and the resulting resonance frequencies are given by

$$\hbar\omega = 6A\left(1 + \frac{\eta^2}{3}\right)^{1/2} \pm \frac{4\xi}{\left(1 + \frac{\eta^2}{3}\right)^{1/2}} + \frac{4\xi^2}{3A\left(1 + \frac{\eta^2}{3}\right)^{3/2}} \frac{\eta^2}{3} \quad (19a)$$

and

$$\hbar\omega = 6A\left(1 + \frac{\eta^2}{3}\right)^{1/2} \pm 2\xi + \frac{4\xi^2}{3A\left(1 + \frac{\eta^2}{3}\right)^{3/2}} \frac{\eta^2}{3} \quad (19b)$$

for any value of η and to the second order in the magnetic field. When the magnetic field is parallel to the z-axis the frequency difference between the inner lines is a maximum (from symmetry considerations of the Zeeman spectra) and is equal to 4ξ .

$$\text{The value of } \eta \cos 2\phi = 3 - \frac{2}{\sin^2 \Theta_0} \quad (20a)$$

may be determined by observing the angle Θ_0 at which the inner and outer lines coincide. Then rotating the system $\frac{\pi}{4}$ radians about the z-axis, the value of

$$-\eta \sin 2\phi = 3 - \frac{2}{\sin^2 \Theta_{\pi/4}} \quad (20b)$$

may be determined. Then

$$\eta = \sqrt{18 - \frac{12}{\sin^2 \Theta_0} + \frac{4}{\sin^4 \Theta_0} - \frac{12}{\sin^2 \Theta_{\pi/4}} + \frac{4}{\sin^4 \Theta_{\pi/4}}} \quad (21)$$

Using equations (20_a), (20_b) and (21) the x and y- principal axes may be found.

For example, once the inner lines of the spectra are identified from a general inspection of the split lines, the crystal can be oriented so that the frequency difference between them is equal to 4ξ . This determines the direction of the z-axis (formula (19b)). In practice this may be difficult, however, the directions of the z-axes in the crystal can often be determined from symmetry considerations.

Once the direction of the z-axis is found the directions of the x-axis and y-axis can be found as mentioned previously by using formulae (20_a), (20_b) and (21). Alternatively, it is possible to rotate the crystal about the z-axis and determine the x-axis and y-axis directions, as well as η , from the maxima and minima of the splitting of the inner components.¹

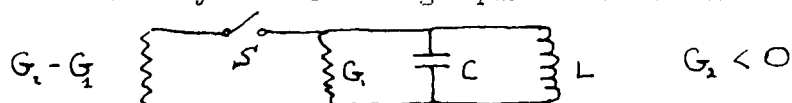
CHAPTER IITHE SUPER-REGENERATIVE OSCILLATOR

Nuclear quadrupole resonances may be observed by placing a suitable crystalline sample in a solenoid which has an oscillating voltage of the proper frequency applied to it. The internal field of the solenoid can be considered as the superposition of two magnetic fields rotating in opposite directions. The sample will absorb energy from the magnetic field by means of the coupling between the magnetic field and the nuclear magnetic dipole moments. Classically, the resonating nuclei can be pictured as precessing around the z-axis of the electric field. About half of the nuclei will tend to be aligned and rotating in one direction while the others will tend to be aligned and rotating in the other direction. Energy will continue to be absorbed as thermal motions tend to dephase the precessing nuclei and if the oscillating voltage is removed the net magnetization will decay with a time constant τ_q characteristic of the sample while it is inducing a voltage in the solenoid. For maximum coupling the axis of the solenoid should be at right angles to the electric field z-axis.

To observe the Zeeman splitting of nuclear quadrupole resonances the sample must be a single crystal because of the frequency dependence of the split lines with angle between the electric field z-axis and the applied magnetic field. Also, since the magnetic field removes the $\pm m_z$ degeneracy of the energy levels, only one rotating component of the solenoid field will cause the nuclei to precess. This is the same as in nuclear magnetic resonance.

In practice this solenoid forms part of a tuned circuit tuned at the resonance frequency and the production of the oscillating voltage and the observation of the resonance can be accomplished by a super-regenerative oscillator. A super-regenerative oscillator is an ordinary oscillator which has a periodic voltage applied to one of its electrodes so that the oscillations occur in bursts. This periodic voltage is called the quench voltage.

An idealized super-regenerative oscillator using a square wave quench voltage can be described by the following equivalent circuit



L, C, G_1 represent the tuned circuit and L is the sample coil. The oscillator circuit may be adjusted so that the conductance supplied by the tube, $G_2 - G_1$ is negative.

The action of a square wave quench voltage of period T is to open and close the switch S . When the switch is closed at $t = 0$ the oscillations will be given by

$$v_a(t) = V_0 e^{-\alpha_2 t} \cos\left(\frac{1}{Lc} - \alpha_2^2\right)^{\frac{1}{2}} t \quad (22a)$$

$$0 \leq t \leq \frac{T}{2}$$

where

$$\frac{G_1}{2C} \equiv \alpha_1 > 0 \quad ; \quad \frac{G_2}{2C} \equiv \alpha_2 < 0$$

When the switch is opened at time $\frac{T}{2}$ the oscillations will be given by

$$v_b(t) = V_0 e^{-\alpha_1 \frac{T}{2}} e^{-\alpha_1 (t - \frac{T}{2})} \cos\left(\frac{1}{Lc} - \alpha_1^2\right)^{\frac{1}{2}} \left(t - \frac{T}{2}\right) \quad (22b)$$

$$\frac{T}{2} < t \leq T$$

If $\frac{T}{2}$ is long enough, the oscillator will saturate and the envelope of the

oscillations will become flat with a constant voltage $V_a(\frac{T}{2})$. This mode of operation is depicted in Figures 2 and 3.

If at time T

$$V_a(\frac{T}{2}) e^{-\alpha \frac{T}{2}} > V_n \quad (23)$$

where V_n is the average amplitude of the noise voltage in the tuned circuit the oscillations will start up again from this voltage $V_b(T)$ and coherent operation will result. (Figure 2a.). However, if $V_b(T)$ is much less than V_n then the oscillations will start up from the randomly phased noise voltage present and incoherent bursts of oscillations will result (Figure 2b.).

The frequency spectrum of the oscillator energy is a Fourier transform of the time variation of the energy present in the tuned circuit. Without a sample, in the coherent state the frequency spectrum consists of a central line with a number of sidebands separated by the quench frequency. (Figure 2c.). As the tuned circuit is varied in frequency the set of lines will shift accordingly in frequency.

In the incoherent state the frequency spectrum is a continuous noise spectrum with the shape that of the frequency response curve of the tuned circuit to a first approximation and the half-power points are separated by the bandwidth B_1 , of the tuned circuit (Figure 2d.) where

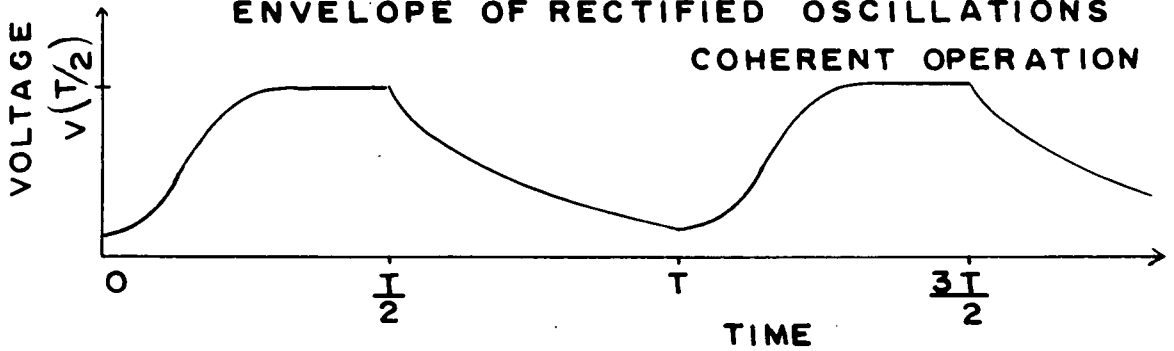
$$B_1 = G_1 / 2\pi C$$

corresponding to a noise bandwidth

$$B_n = G_1 / 4C$$

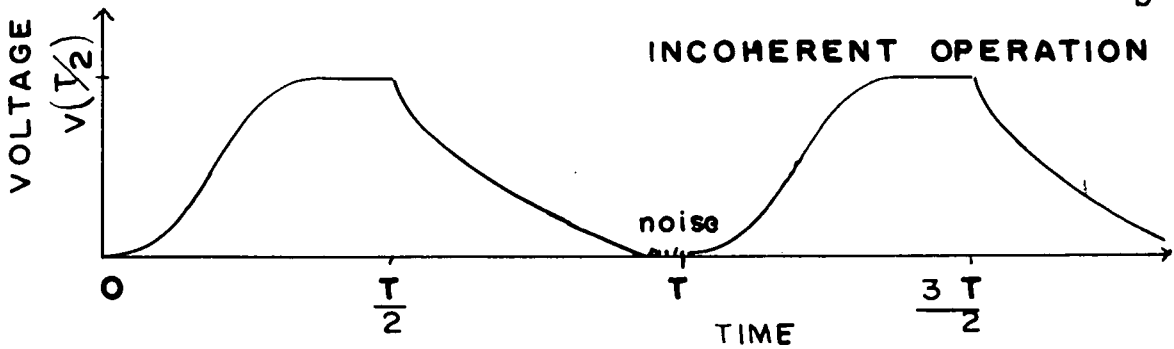
Also as the tuned circuit is varied in frequency the peak of the noise spectrum shifts accordingly in frequency.

FIGURE 2
ENVELOPE OF RECTIFIED OSCILLATIONS
COHERENT OPERATION



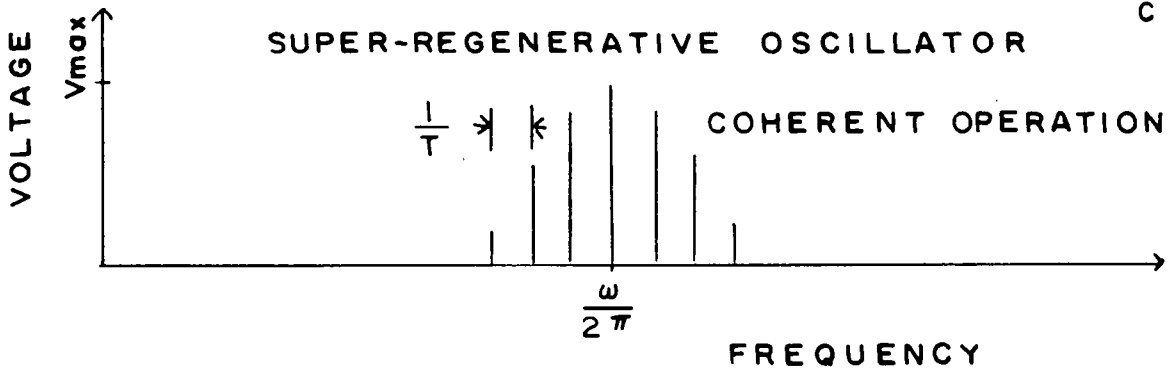
b

INCOHERENT OPERATION



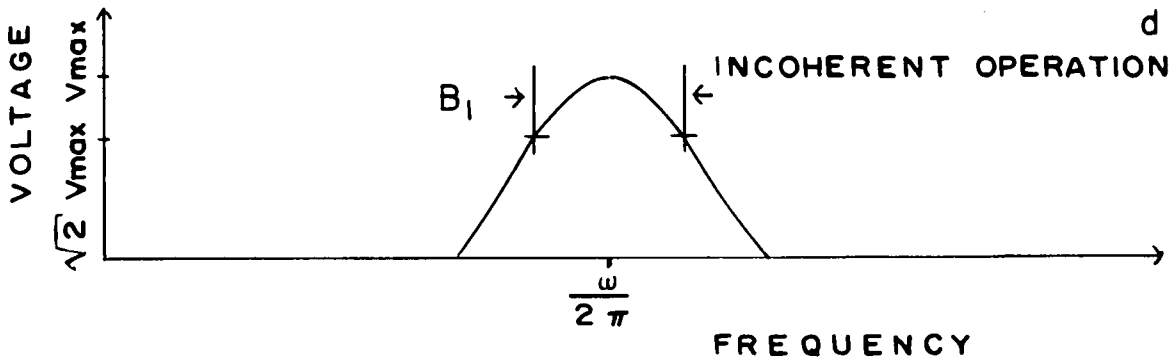
RECTIFIED OUTPUT OF
SUPER-REGENERATIVE OSCILLATOR

c



d

INCOHERENT OPERATION



OPERATION OF SUPER-REGENERATIVE OSCILLATOR WITH NO
SAMPLE PRESENT

The behaviour of the super-regenerative oscillator which, without a sample is operating in the incoherent state, is somewhat different with a sample present in the solenoid. When the switch \mathcal{S} is closed at $t = 0$ the oscillations build up and energy is absorbed by the sample and the nuclei caused to precess as described previously. When the switch is opened at $t = \frac{\tau}{2}$ there is, in addition to the voltage given by equation (21b), a voltage induced by the precessing nuclei

$$V_s(t) = V_s\left(\frac{\tau}{2}\right) e^{-\frac{(t - \frac{\tau}{2})}{\tau_Q}} \cos \omega_Q(t - \frac{\tau}{2}) \quad (24)$$

where ω_Q is the frequency of the nuclear quadrupole resonance.

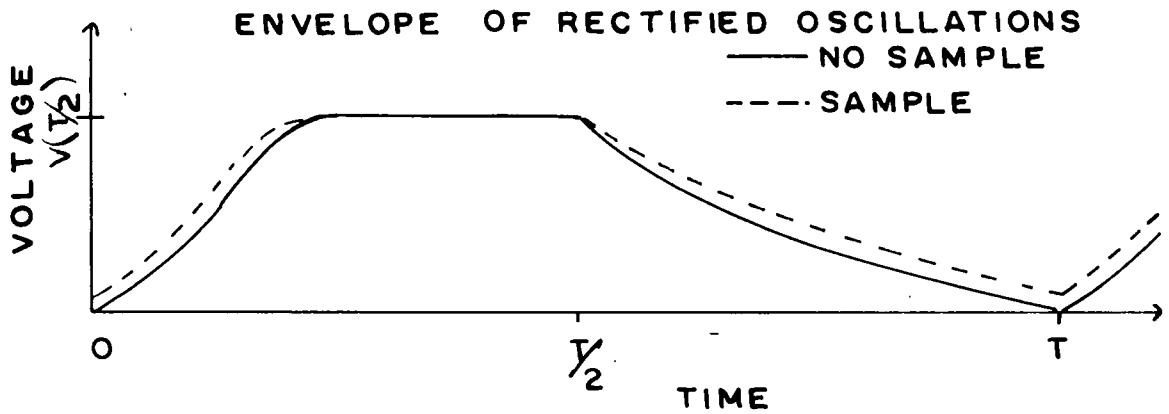
At time τ the oscillations will start up from this voltage and coherent oscillations will result with the frequency of oscillation determined by ω_Q . The radiated energy has a frequency spectrum similar to that for coherent operation without a sample except that as the tuned circuit is varied in frequency the center line and sidebands stay constant in frequency but their amplitudes will change because of the tuned circuit frequency response. (Figure 3.).

The relaxation time of the sample τ_Q must not be too short otherwise the signal V_s will be less than the noise voltage V_n and incoherent operation will result. The most sensitive point of operation would seem to be that where, without a sample, the super-regenerative oscillator is almost entering the coherent state. This point can be reached by adjusting various circuit parameters such as feedback, quench voltage and frequency, and electrode potentials.

The signal to noise ratio of a resonance will be determined by the signal voltage across the resistor $(G_1)^{-1}$, as well as the effective noise voltage per unit bandwidth $^{\frac{1}{2}}$ across G_1 and the effective noise bandwidth B_n of the detection

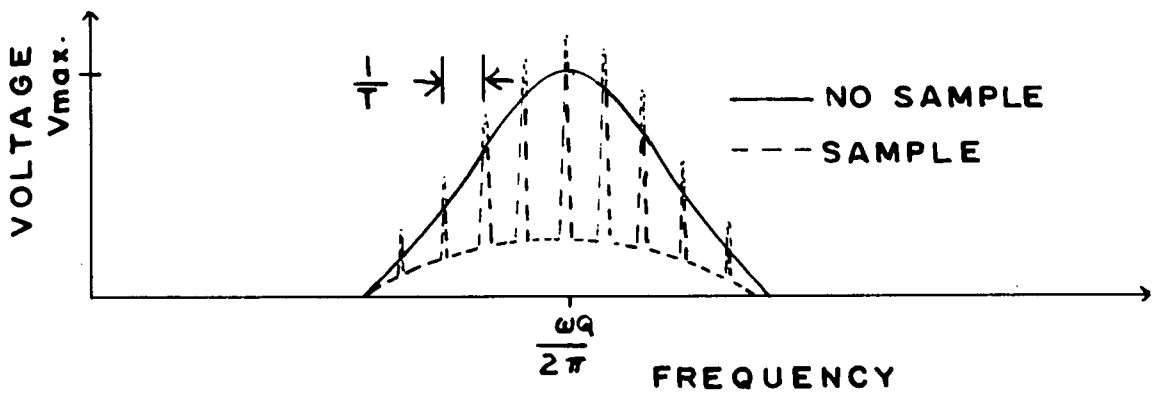
FIGURE 3

to follow page 13
a



b

RECTIFIED OUTPUT OF
SUPER-REGENERATIVE OSCILLATOR



EFFECT OF SAMPLE UPON SUPER-REGENERATIVE
OSCILLATOR OPERATION

system. Since the signal voltage is

$$V_s(t) = V_s\left(\frac{T}{2}\right) e^{-\frac{\pi}{2\tau_a}} \cos \omega_Q \left(t - \frac{T}{2}\right) \quad (24)$$

the mean square signal voltage is

$$\overline{V_s^2} = \frac{V_s^2\left(\frac{T}{2}\right)}{2} e^{-\frac{\pi}{\tau_a}}$$

and the mean square noise voltage is

$$\overline{V_n^2} = k T_{\text{eff}} / C = 4k T_{\text{eff}} B_n / G_1$$

where

k is Boltzmann's constant

T_{eff} is the effective temperature of the noise present in the system.

The value of T_{eff} is given by the temperature of a resistor that will produce the same available noise power per unit bandwidth as the system does since, over a small frequency range, the system noise power per unit bandwidth is constant.

Part of this system noise is produced by the conductance G_1 which usually is at room temperature. The temperature of the noise produced by the tube depends upon its operation. A tube when operated as a super-regenerative oscillator is probably somewhat noisier than when it is operated as an amplifier since, as with a mixer, it is not operated at its least noisy point at all times. An external quench oscillator can introduce noise since variations in the quench frequency (assuming a square wave quench voltage) will cause variations in the starting up time of the oscillations and hence add a certain incoherence in them.

If the detection process takes place in the super-regenerative oscillator circuit and the detected signal passed through an audio amplifier of effective noise bandwidth B_n AF the signal to noise ratio is

$$\begin{aligned} \frac{\overline{V_s^2}}{V_n^2} &= \frac{1}{2} \frac{C V_s^2(\frac{T}{2})}{R T_{eff}} e^{-\frac{T}{\tau_q}} \left(\frac{B_n}{B_{nAF}} \right)^{1/2} \\ &= \frac{1}{8} \frac{V_s^2(\frac{T}{2})}{R T_{eff}} e^{-\frac{T}{\tau_q}} \frac{G_1}{(B_n B_{nAF})^{1/2}} \end{aligned} \quad (25)$$

In the case where $B_{nAF} \gg B_n$ the effective noise bandwidth of the system is B_n . For best results the quench period T is

$$T = \frac{\text{constant}}{B_n} = \frac{K}{B_n} = \frac{2}{\pi} \frac{K}{B_n}$$

Where the constant K is chosen so that the oscillations in the tuned circuit without a sample will just die down below the noise level before the next cycle begins.

$$\frac{\overline{V_s^2}}{V_n^2} = \frac{1}{8} \frac{V_s^2(\frac{T}{2})}{R T_{eff}} \frac{\pi}{2} \frac{G_1}{K} T e^{-\frac{T}{\tau_q}}$$

This expression is a maximum for

$$T = \tau_q$$

and the signal to noise ratio is

$$\frac{\overline{V_s^2}}{V_n^2} = \frac{1}{8} \frac{V_s^2(\frac{T}{2})}{R T_{eff}} \frac{\pi}{2} \frac{G_1}{K} \frac{\tau_q}{e} \quad (26)$$

Therefore, for optimum circuit constants, the signal to noise ratio will be proportional to the decay time τ_q of the sample.

Alternatively, it is possible to amplify the signal radiated by the super-regenerative oscillator, filter it through an effective noise bandwidth B_{nRF} detect it, and pass it through an audio filter of effective noise bandwidth B_{nAF} . B_{nRF} is assumed to be less than $\frac{1}{T}$ and $B_{nAF} \leq B_{nRF}$. The signal to noise ratio is

$$\frac{\overline{V_s^2}}{V_n^2} = \frac{1}{8} \frac{V_s^2(\frac{T}{2})}{R T_{eff}} e^{-\frac{T}{\tau_q}} \frac{G_1}{((1+\delta) B_{nRF} B_{nAF})^{1/2}} \quad (27)$$

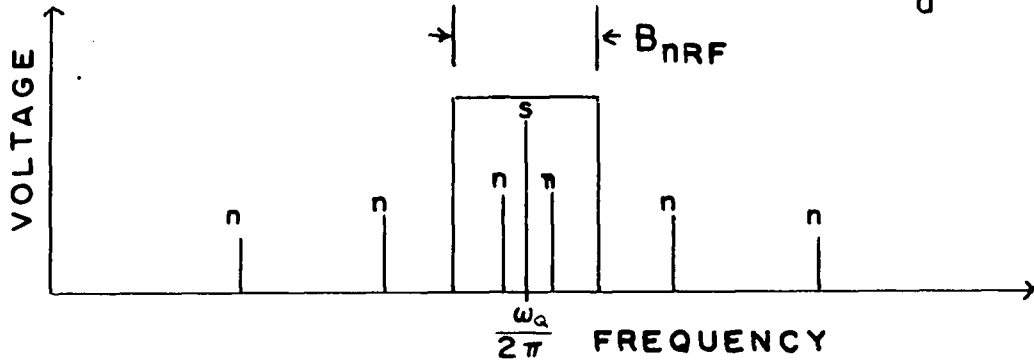
The factor $(1+\delta)$ arises in the denominator because when the super-regenerative oscillator is operating in the coherent state with a sample in the solenoid it can be considered as an amplitude modulated oscillator where the modulation is a complex combination of sine waves of periods $\frac{T}{2\pi n}$ where n is integral. Therefore, signal voltage will be modulated and possess several sidebands on either side of the signal frequency spaced by the quench frequency (Figure 4b.) The noise can be considered as several (infinitely many) noise voltages with instantaneous frequencies spread throughout the spectrum determined by the tuned circuit of the Super-regenerative oscillator (Figure 4a.). Hence each noise voltage will have several sidebands on either side of the instantaneous frequency and spaced by the quench frequency.

The effect of the modulation is to place more noise voltages within the noise bandwidth $B_n RF$ (Figure 4c.). The noise voltages add incoherently so that the increase in noise power may be described by δ where δ depends upon the complex modulation and the shape of the tuned circuit response curve. If a large enough bandwidth $B_n RF \approx \frac{\pi}{2} B_1$ is used then all the energy radiated by the Super-regenerative oscillator is accepted and the presence of the quench voltage has no effect on the signal to noise ratio which will then be that given in equation (25).

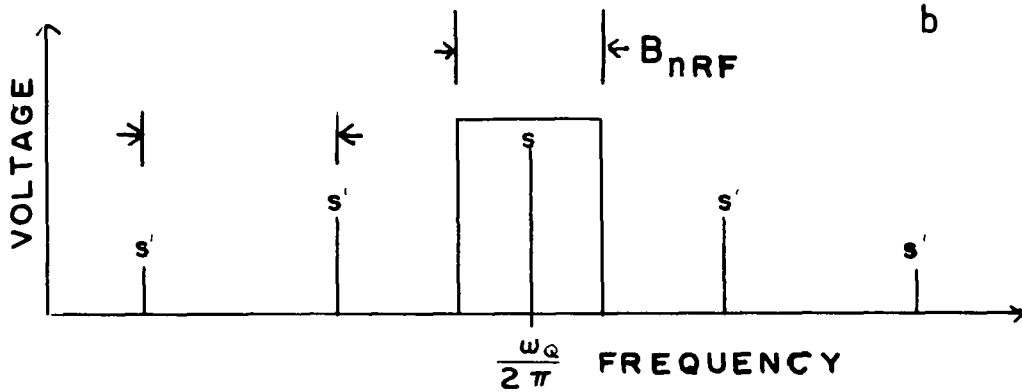
For very weak signals, maximum sensitivity is obtained using some form of phase-sensitive detection. Usually in this method of detection the signal is modulated at an audio frequency with the modulation being detected and then passed into a phase-sensitive mixer whose local oscillator signal is taken from the modulation oscillator with a possible phase change. A direct current out-

FIGURE 4 to follow page 16

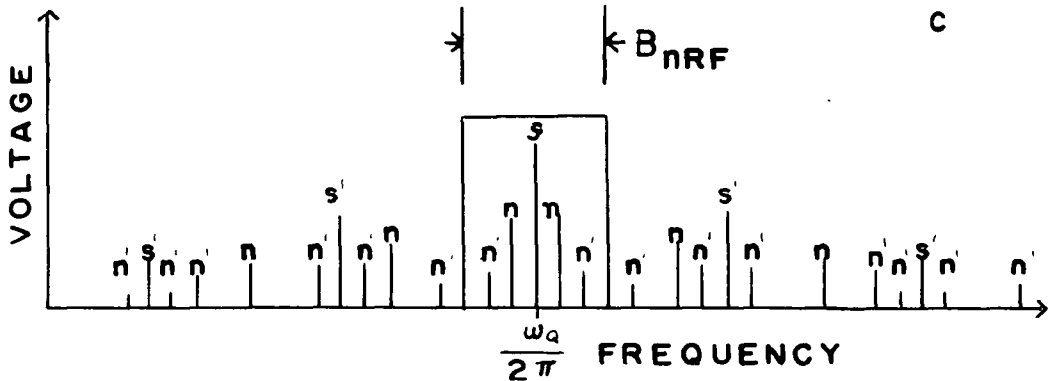
SIGNAL AND NOISE



MODULATED SIGNAL



MODULATED SIGNAL AND NOISE



EFFECT OF THE QUENCHING PROCESS ON THE SIGNAL TO NOISE RATIO OF THE SEPARATE DETECTION METHOD

put is obtained and passed through a resistance-capacitance filter of time constant $\tau_{D.C.}$ and then displayed with an ammeter. Because of the large local oscillator voltage present at the phase-sensitive mixer the effective noise bandwidth is

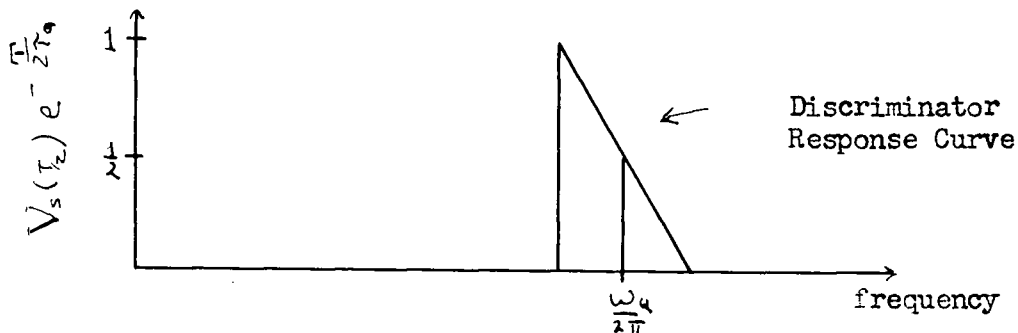
$$\begin{aligned} B_{n\text{ DC}} &= \text{two times the effective noise bandwidth of a single} \\ &\text{stage R-C filter} \\ &= 2 \times \frac{1}{4\tau_{D.C.}} = \frac{1}{2\tau_{D.C.}} \end{aligned}$$

The factor two occurs since both the upper and lower noise sidebands resulting from the mixing process contribute to the noise output. Therefore, we have

$$\frac{\overline{V_s^2}}{\overline{V_n^2}} = \frac{1}{8} \frac{\overline{V_s^2}(\frac{\pi}{2})}{R T_{\text{eff}}} e^{-\frac{\pi}{\tau_Q}} \frac{2\tau_{D.C.} G_1}{(1+\delta)} \quad (28)$$

In the case where the signal is frequency modulated and the modulation recovered by passing the signal through a linear frequency discriminator the signal voltage may be represented by

$$V_s(t) = \overline{V_s}(\frac{\pi}{2}) e^{-\frac{\pi}{2\tau_Q}} \frac{1}{2} (1 + m \cos \omega_m t) \cos \omega_Q t$$



The factor $\frac{1}{2}$ occurs since the undeviated signal is kept at the mid-point of the discriminator curve. The factor $m \leq 1$ allows for the frequency deviation of the signal being less than the width of the frequency discriminator curve.

When this voltage is passed through a quadratic detector where

$$V_{\text{out}}(t) = D V_{i_n}^2(t)$$

the output voltage is

$$\begin{aligned} V_{out}(t) &= D \widehat{V_{in}^2}(t) \\ &= D \frac{m}{4} V_s^2 \left(\frac{T}{2}\right) e^{-\frac{T}{\tau_q}} \cos \omega_m t \quad (29a) \end{aligned}$$

where $\widehat{\quad}$ means a time average long compared to $\frac{1}{\omega_q}$ but short compared to $\frac{1}{\omega_m}$.

Without modulation the direct current output signal voltage would be

$$V_{out} = D \frac{V_s^2}{2} \left(\frac{T}{2}\right) e^{-\frac{T}{\tau_q}} \quad (29b)$$

With $m=1$ the coefficient of the $\cos \omega_m t$ output (29a) is equal to $\frac{1}{2} V_{out}$ given by (29b). If the spectral density of the noise power is independent of frequency over the range which the signal is deviated, then frequency modulation of the noise produces no extra noise output at the modulation frequency after being passed through a frequency discriminator and a quadratic detector. Therefore, this particular type of recovery of frequency modulation reduces the signal to noise ratio by a factor of two assuming equal effective noise bandwidths in each case.

The maximum signal to noise ratio will be most easily obtained by using a phase-sensitive detection system with a direct current filter of long time constant while using as high a quench frequency as possible.

CHAPTER IIITHE NUCLEAR QUADRUPOLE RESONANCE SPECTROMETER

The basis of the spectrometer is a push-pull grounded-grid super-regenerative oscillator with cathode quench voltage injection using type 955 acorn triode tubes. The tuned circuits are shorted parallel wire transmission lines. The cathode line is adjusted to give the proper feedback and the plate line, which has the sample coil in parallel with it, determines the frequency of operation of the oscillator.

The value of T_{eff} is assumed to be of the order of a few thousand degrees Kelvin when the system is operated at 150 mc/s. The tuned circuit bandwidth B_1 is of the order of 300 kc/s at this frequency. The quench frequency is normally 50 kc/s.

If the detection process takes place in the super-regenerative oscillator circuit the signal can be amplified and displayed on an oscilloscope with the oscillator frequency modulated using a vibrating condenser and the oscilloscope swept in synchronism with the frequency changes. Since the feedback, which is controlled by the tuning of the cathode line, does not have to be changed over a fairly wide frequency range of plate line tuning the spectrometer is suitable for searching for nuclear quadrupole resonances. For maximum sensitivity in searching, phase-sensitive detection may be used where the resonance is modulated by using a Zeeman modulation field supplied by a set of small Helmholtz coils.⁴

The disadvantage of the self-detection process is that the adjustments

are much more critical than when the detection is accomplished separately. It also tends to be unsuitable for observing Zeeman splittings of nuclear quadrupole resonances since the resolution is essentially determined by the bandwidth B_1 of the tuned circuit. Greater resolution can be obtained by amplifying the radiated signal from the super-regenerative oscillator and passing it through a filter of bandwidth B_{RF} which determines the resolution and then detecting the resonance.

The radiation of the super-regenerative oscillator is fed to a balanced germanium diode crystal mixer through capacitive coupling consisting of a short length of wire situated near the super-regenerative oscillator tuned circuit. The local oscillator voltage is supplied to the mixer by a triode frequency tripler stage excited by a quartz crystal controlled oscillator (Figure 6a.). The difference frequency is fed into a Hammurlund HQ-129-X communications receiver. The difference frequency is determined by a BC-221-A frequency meter. The receiver is equipped with a crystal filter so that the bandwidth B_{RF} can be varied from a few hundred to a few thousand c/s. $B_n RF$, the noise bandwidth, is of the same order. The nuclear quadrupole resonance which appears as a series of noisy peaks separated by the quench frequency at the output of the receiver can be heard with earphones or it may be rectified and displayed with an ammeter (Figure 5a.).

Since the signal from the super-regenerative receiver into the mixer is large no extra noise is introduced by the rest of the spectrometer. The rectified noise voltage at the output of the receiver was found to vary inversely as the quench frequency over a wide range of quench frequencies.

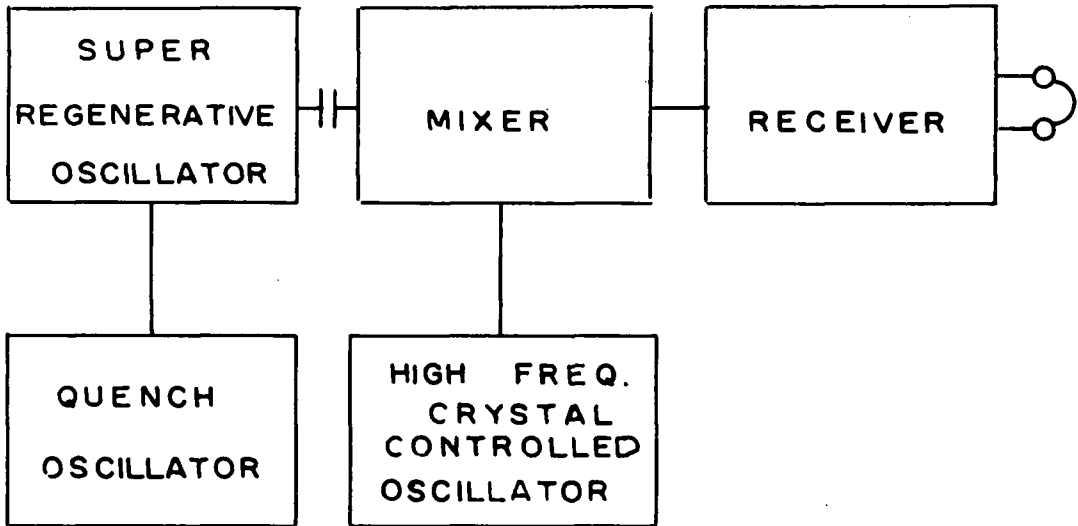
In practice, when observing the Zeeman splitting of the resonances, the

FIGURE 5

to follow page 20

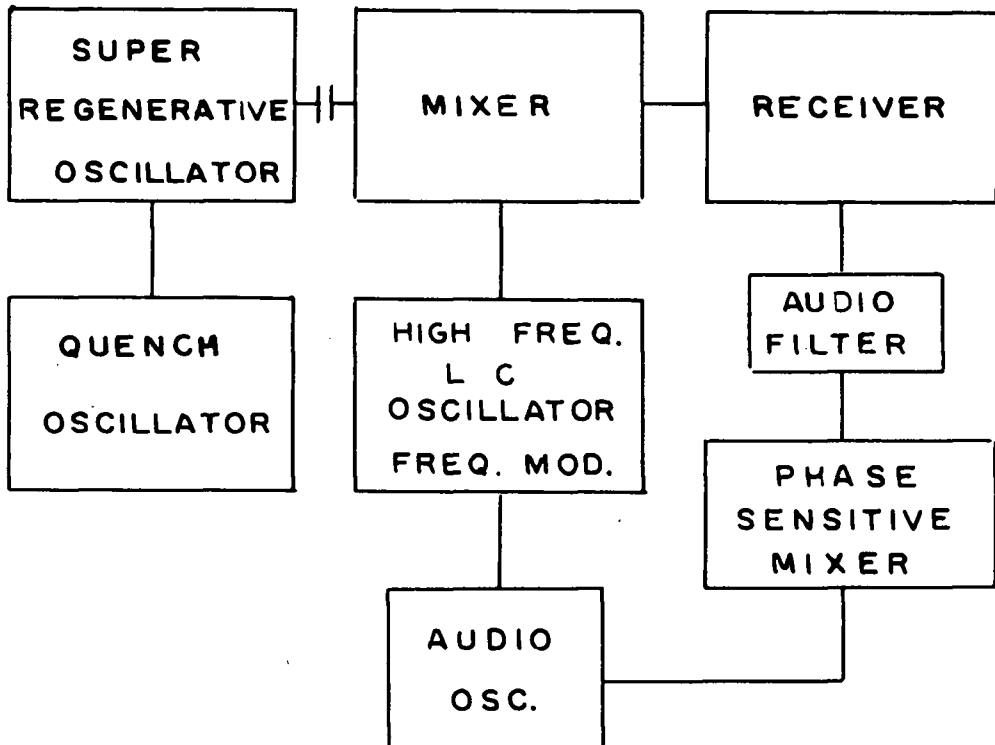
SEPARATE DETECTION

a



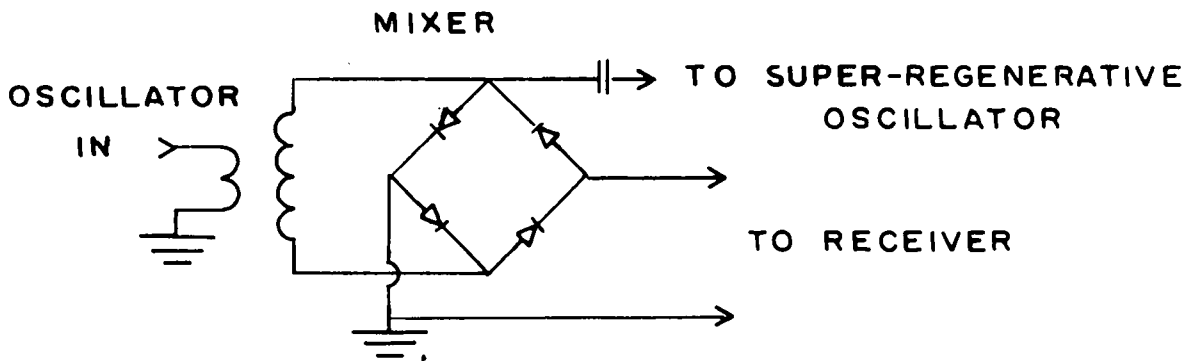
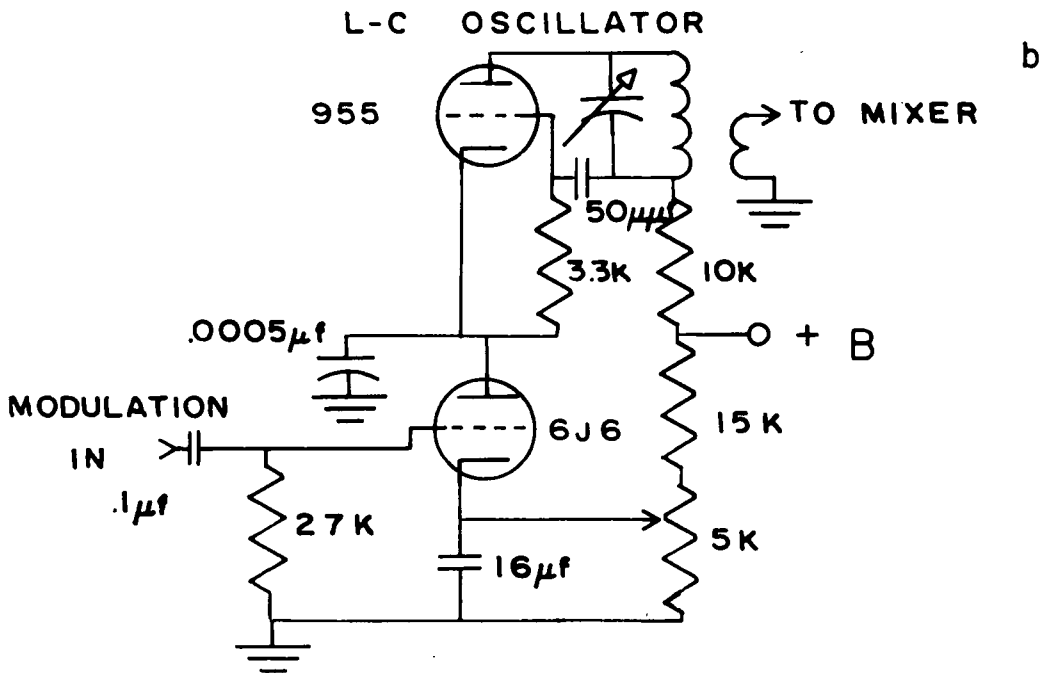
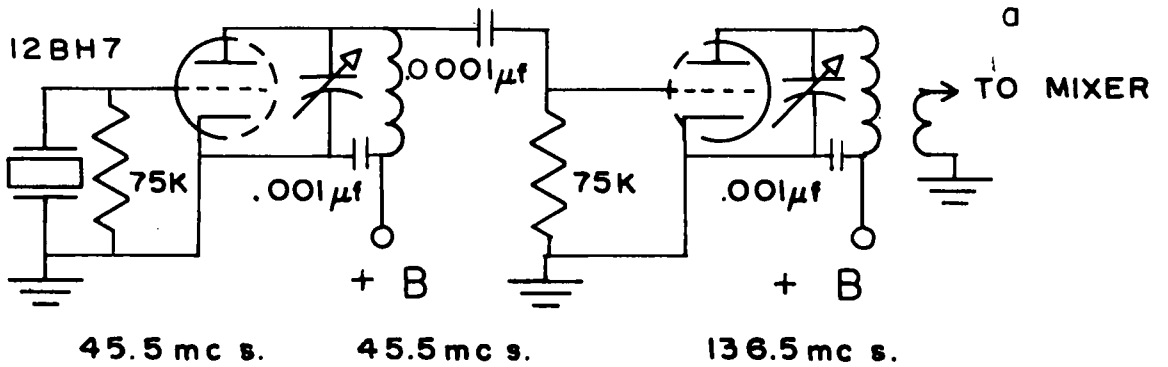
b

PHASE SENSITIVE DETECTION



BLOCK DIAGRAMS OF THE APPARATUS

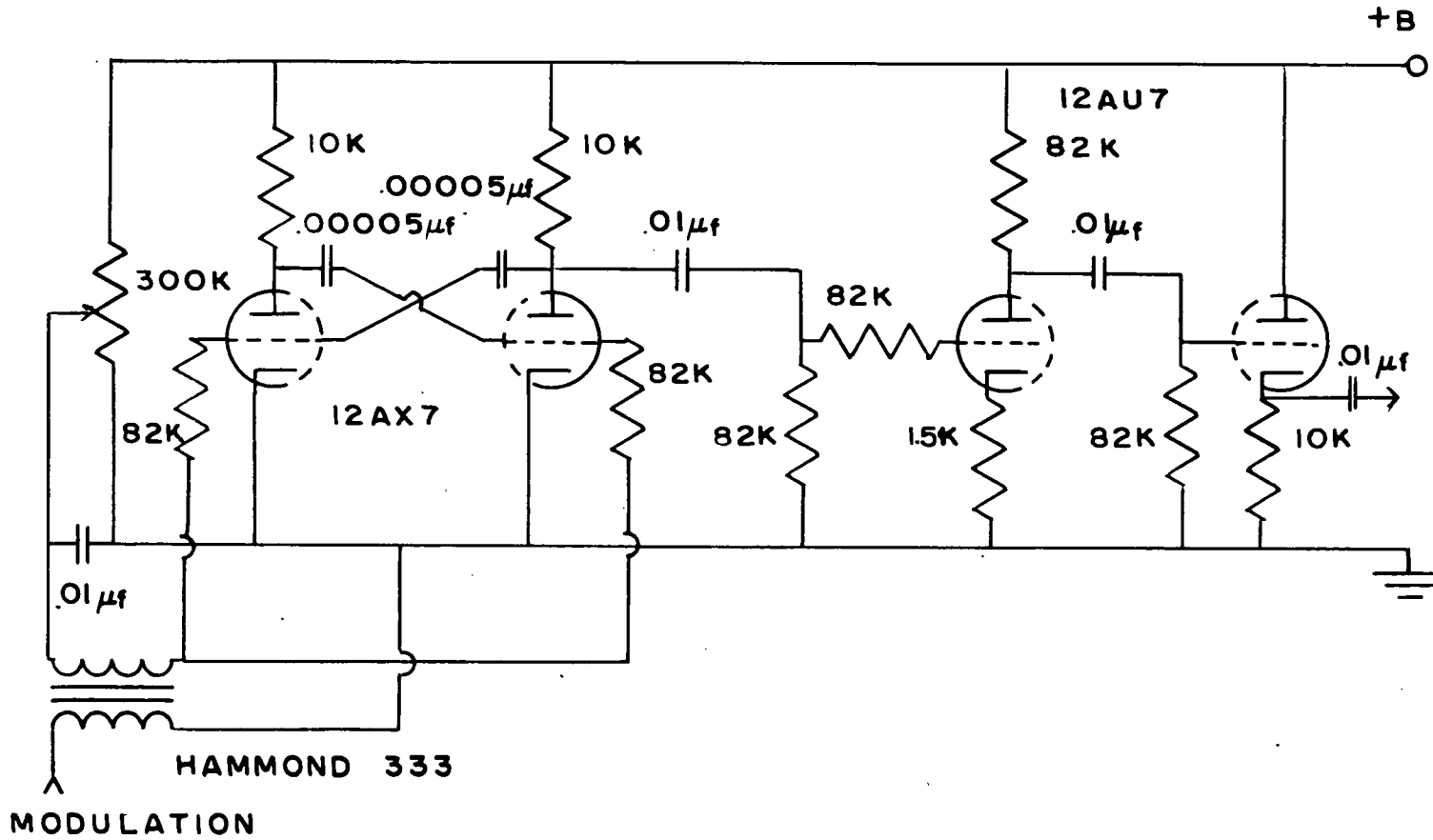
FIGURE 6 to follow page 20
CRYSTAL CONTROLLED OSCILLATOR & TRIPLER



WIRING DIAGRAMS

FIGURE 7 to follow page 20

FREQUENCY MODULATED QUENCH OSCILLATOR



WIRING DIAGRAM

receiver is set to a given frequency with the aid of the frequency meter, and the super-regenerative oscillator tuned for maximum noise at the receiver output. The crystal is rotated in the magnetic field and, since the local oscillator frequency is known, the frequency of the resonance as a function of crystal orientation in the magnetic field may be determined. Since there are several peaks for each resonance the center line can be found by changing the quench frequency since only the central line will remain unchanged in frequency. If the resonance is fairly strong, a frequency modulated quench oscillator may be used and the resulting unmodulated center line picked out quickly (Figure 7.).

For more sensitivity phase-sensitive detection is used. Modulation of the signal is obtained by modulating the high frequency oscillator and is recovered by sweeping the resonance back and forth over one side of the receiver response curve. The resulting variations are filtered and passed into the phase sensitive mixer, the signal being displayed on an Esterline-Angus graphic meter. A time constant $\tau_{D.C.}$ of three seconds is usually used. (Figure 5b.)

Suitable frequency modulation of the crystal controlled oscillator was not obtained and amplitude modulation of this oscillator has the disadvantage that the noise is modulated also, introducing a D.C. component when passed into the phase-sensitive detector. The long term D.C. stability was not good enough for the weak signals encountered. Instead, another local oscillator was used where the frequency was determined by an ordinary tuned circuit. The plate voltage was modulated slightly causing the resulting local oscillator signal to be almost entirely frequency modulated. The second harmonic was used for mixing. (Figure 6b.).

Modulation of the magnetic field could be used when Zeeman split resonances are observed but the frequency deviation of the resonance is proportional to the splitting and in some cases a resonance would not be observed.

The main magnetic field is supplied by a set of water cooled Helmholtz coils. Each coil has a bobbin with a winding space of 50 mm by 50 mm filled with #14 B. and S. gauge enamel covered copper wire. This gives 620 turns. The wire is spaced every two layers by thin strips of card and the bobbin has holes punched in the sides to allow a free flow of cooling water. The bobbin has a brass ring for the center and another brass ring is slipped over the outer edge. Circular Tufnol plates with grooves and neoprene washers are placed on either side and held together with long bolts to make a water tight jacket. The inlet and outlet pipes for the water also act as terminals for the coils.

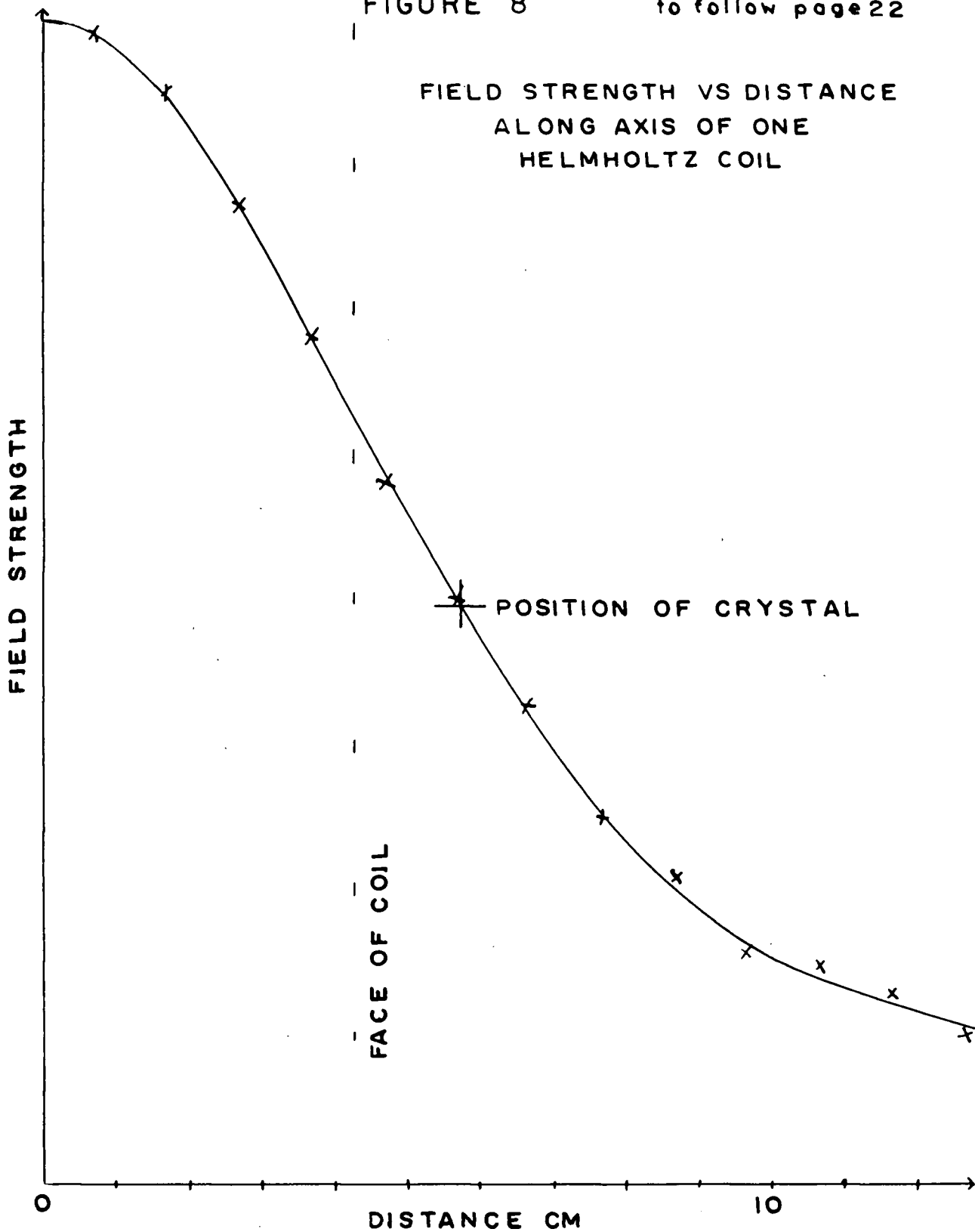
The field strength along the axis of one of the coils was measured using a flux meter and a graph (Figure 8.) drawn to determine the position of most nearly linear variation of field strength with distance, i.e. the point of inflexion of the curve. The graph indicated that the two coils should be placed as close together as possible. The spacing was actually limited by the projection of the outlet pipes from the inner faces.

The crystal holder is mounted on a rotating shaft and the supporting post which acts as a bearing is attached to the base of the Helmholtz coils. The crystal holder, shaft, and post are made of lucite to avoid distorting the magnetic field near the crystal. The system was aligned in order to have the axis of rotation as nearly normal to the magnetic field as possible. At a current of 25 amperes through each coil the field at the crystal is 1.4 kilogauss and little heating of the coils is noticed.

FIGURE 8

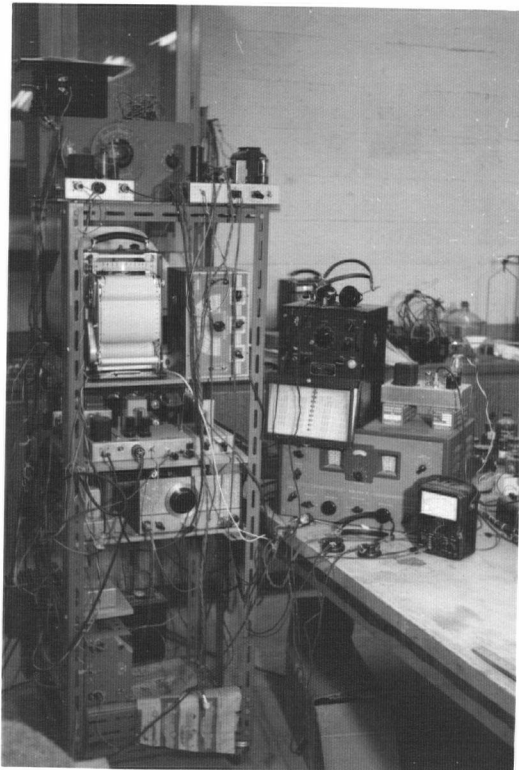
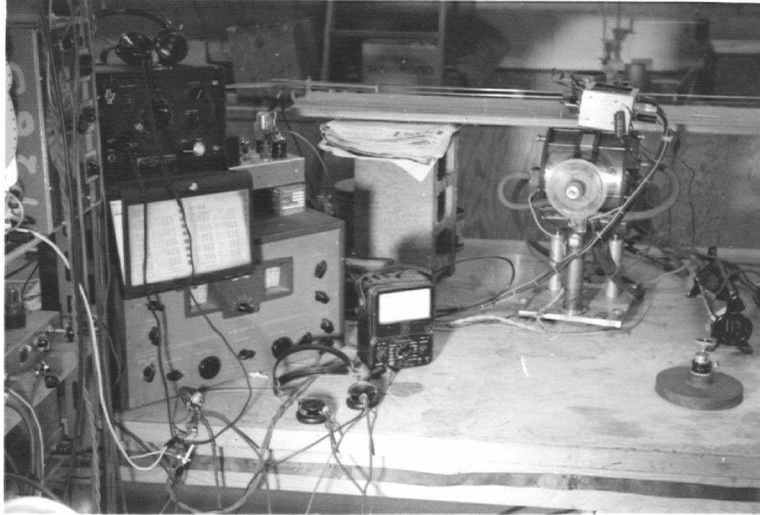
to follow page 22

FIELD STRENGTH VS DISTANCE
ALONG AXIS OF ONE
HELMHOLTZ COIL



THE SPECTROMETER

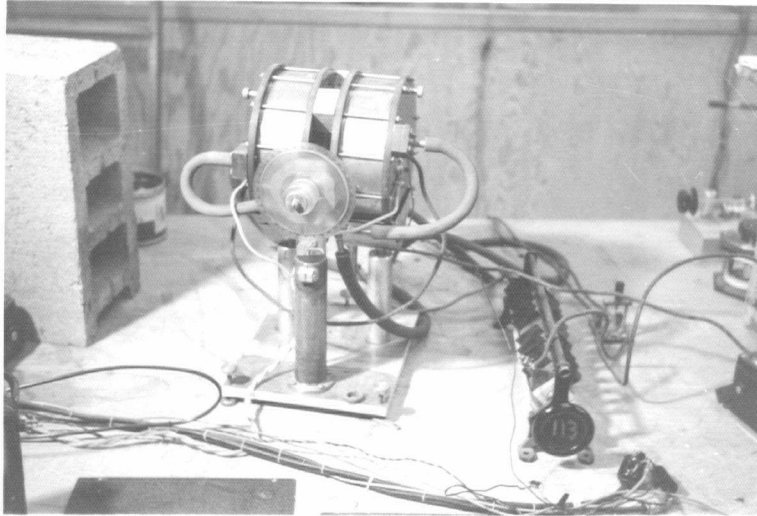
SEP • 59 •



SEP • 59 •

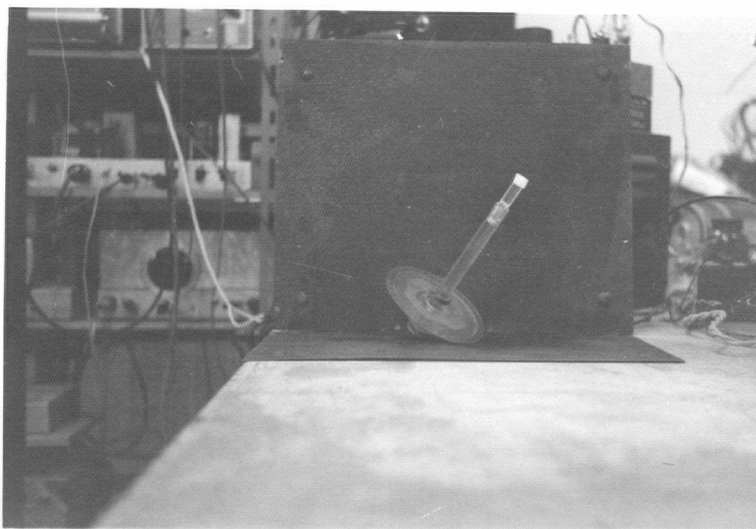
HELMHOLTZ COILS

SEP • 59



CRYSTAL HOLDER

SEP • 59 •



CHAPTER IVINFORMATION OBTAINED ABOUT SINGLE CRYSTALS
OF $Zn(BrO_3)_2 \cdot 6H_2O$ AND $Co(BrO_3)_2 \cdot 6H_2O$ FROM
THEIR ZEEMAN SPECTRA.

The Zeeman splitting of the nuclear quadrupole resonances of single crystals of $Zn(BrO_3)_2 \cdot 6H_2O$ and $Co(BrO_3)_2 \cdot 6H_2O$ were observed. The crystals were grown by evaporating an aqueous solution of the salt from a beaker in which a seed crystal had been placed. The resulting crystals had volumes of about one cubic centimeter.

The lucite crystal holders were turned on a lathe so that the face would be normal to the axis of rotation of the shaft. The crystals were usually attached by gluing one crystal face to the holder with a thin layer of polystyrene glue, which had the advantage that the crystal could be pried off easily without damage and could be remounted with a different orientation in the magnetic field. If necessary lucite shims could be used to mount the crystal in any given position.

The current for the Helmholtz coils was supplied by a generator and was kept at a constant value of $25.00 \pm .05$ amperes by means of a high-wattage variable carbon compression resistor. Care had to be taken to avoid the magnetic field from the Helmholtz coils affecting the reading of the D.C. ammeter used to measure the magnet current.

Since most unsplit resonance frequencies of the Br^{81} isotope in the metallic bromates lie in the 140 mc/s to 150 mc/s range a 45.5 mc/s quartz crystal was used so that the resulting frequency of $136.500 \pm .015$ mc/s allowed

a convenient difference frequency to be accepted by the receiver. Absolute frequency measurements were estimated to be accurate to within ± 20 kc/s. Relative frequency measurements where the receiver was set at a given frequency with the frequency meter and then used to determine the resonance frequencies were estimated to be accurate within ± 5 kc/s over periods of an hour or so.

In practice the measured unsplit resonance frequency did not show this stability. Variations in the quench voltage and frequency and variations of the tuned circuit frequency of the super-regenerative oscillator would change the central line frequency by as much as ± 20 kc/s. Daily variations in the central line frequency amounted to as much as ± 30 kc/s.

Although it is assumed in Chapter II that the super-regenerative oscillator does not react on the sample, by "pulling" the nuclear quadrupole resonance frequency, for example, it may do so to a small extent but the main source of error is believed to lie in the dependence of the resonance frequency on the temperature of the sample. The resonance frequency increases about 5 mc/s when the temperature of $Zn(BrO_3)_2 \cdot 6H_2O$ is changed from room temperature to liquid air temperature.

At room temperature the unsplit resonance frequencies of $Zn(BrO_3)_2 \cdot 6H_2O$ and $Co(BrO_3)_2 \cdot 6H_2O$ are $148.028 \pm .025$ mc/s and $147.926 \pm .025$ mc/s respectively for the Br^{81} isotope. The line width (the frequency separation between half-power points) is about 4 kc/s for both substances. When the perturbing magnetic field was applied the line width increased to about 15 kc/s due to inhomogeneities in the magnetic field.

The axis of rotation of the crystal holder was perpendicular to the magnetic field within 0.1° . Since the secular equation for the energy levels

depends upon $\sin^2 \Theta$ (formula (16)) replacing Θ by $-\Theta$ will not change the resultant frequencies. When the samples were rotated 180° the difference between the two observed frequencies was less than 3 kc/s or 0.2% of the amount of the frequency splitting. A right angle was assumed in calculations. The dial on the shaft could be read to 0.2° .

In the case of $\text{Zn}(\text{BrO}_3)_2 \cdot 6\text{H}_2\text{O}$ the positions of the molecules in the unit cell are given by Wyckoff¹⁰.

$$\begin{array}{l} \text{Zn} \quad \quad \quad 000 \quad ; \quad \frac{1}{2}, \frac{1}{2}, 0 \quad ; \quad \frac{1}{2}, 0, \frac{1}{2} \quad ; \quad 0, \frac{1}{2}, \frac{1}{2} \\ \text{Br} \quad \pm \left[u, u, u \quad ; \quad \frac{1}{2}+u, \frac{1}{2}-u, \bar{u} \quad ; \quad \frac{1}{2}-u, \bar{u}, \frac{1}{2}+u \quad ; \quad \bar{u}, \frac{1}{2}+u, \frac{1}{2}-u \right] \\ \text{O} \quad \pm \left[\begin{array}{l} x, y, z \quad ; \quad \frac{1}{2}+x, \frac{1}{2}-y, \bar{z} \quad ; \quad \frac{1}{2}-x, \bar{y}, \frac{1}{2}+z \quad ; \quad \bar{x}, \frac{1}{2}+y, \frac{1}{2}-z \\ z, x, y \quad ; \quad \frac{1}{2}+z, \frac{1}{2}-x, \bar{y} \quad ; \quad \frac{1}{2}-z, \bar{x}, \frac{1}{2}+y \quad ; \quad \bar{z}, \frac{1}{2}+x, \frac{1}{2}-y \\ y, z, x \quad ; \quad \frac{1}{2}+y, \frac{1}{2}-z, \bar{x} \quad ; \quad \frac{1}{2}-y, \bar{z}, \frac{1}{2}+x \quad ; \quad \bar{y}, \frac{1}{2}+z, \frac{1}{2}-x \end{array} \right] \end{array}$$

H_2O similar to O

$$\begin{array}{ll} \text{where} & u = .259 \\ & a_0 = 10.316 \text{ \AA} \end{array} \quad \begin{array}{l} \text{O} (x = .190, y = .145, z = .330) \\ \text{H}_2\text{O} (x = .195, y = .050, z = .035) \end{array}$$

Because of the 3-fold symmetry about the Br-Zn-Br axis, the electric field Z-axes should have direction cosines $\left\{ \frac{1}{\sqrt{3}}, \frac{1}{\sqrt{3}}, \frac{1}{\sqrt{3}} \right\}$ and the asymmetry should be zero. The four Z-axes are parallel to the $\{1, 1, 1\}$ crystal axes.⁷

A crystal of $\text{Zn}(\text{BrO}_3)_2 \cdot 6\text{H}_2\text{O}$ was mounted with a $(1, 1, 1)$ face perpendicular to the axis of rotation and a plot of the frequencies of the split lines versus the dial reading of the shaft dial was made. (Figure 10). Formula (15) was used with $\cos \Theta$ replaced by $\sin \alpha \cos \gamma$

$$\nu \omega = \pm 3 \xi \sin \alpha \cos \gamma \pm \xi (4 - 3 \sin^2 \alpha \cos^2 \gamma)^{1/2} \quad (30)$$

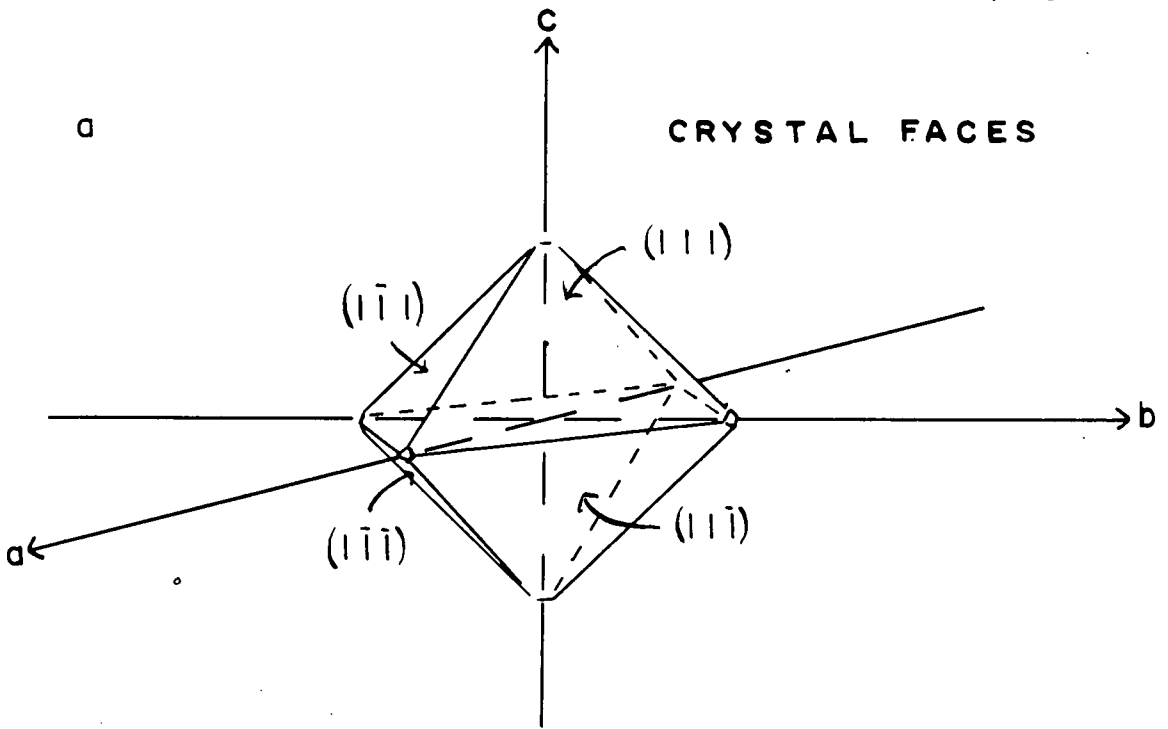
where γ is the dial reading

α is the angle between the z-axis and the axis of rotation

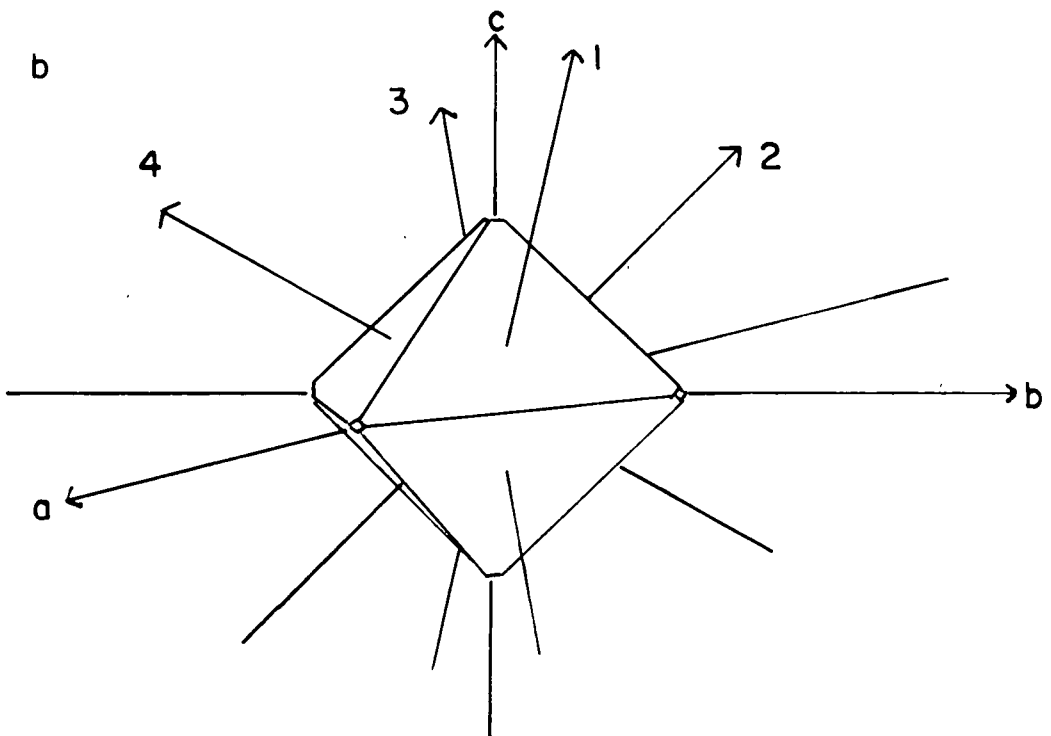
$$\sin \alpha = \frac{\sqrt{8}}{3} \text{ from symmetry considerations.}$$

FIGURE 9

to follow page 25

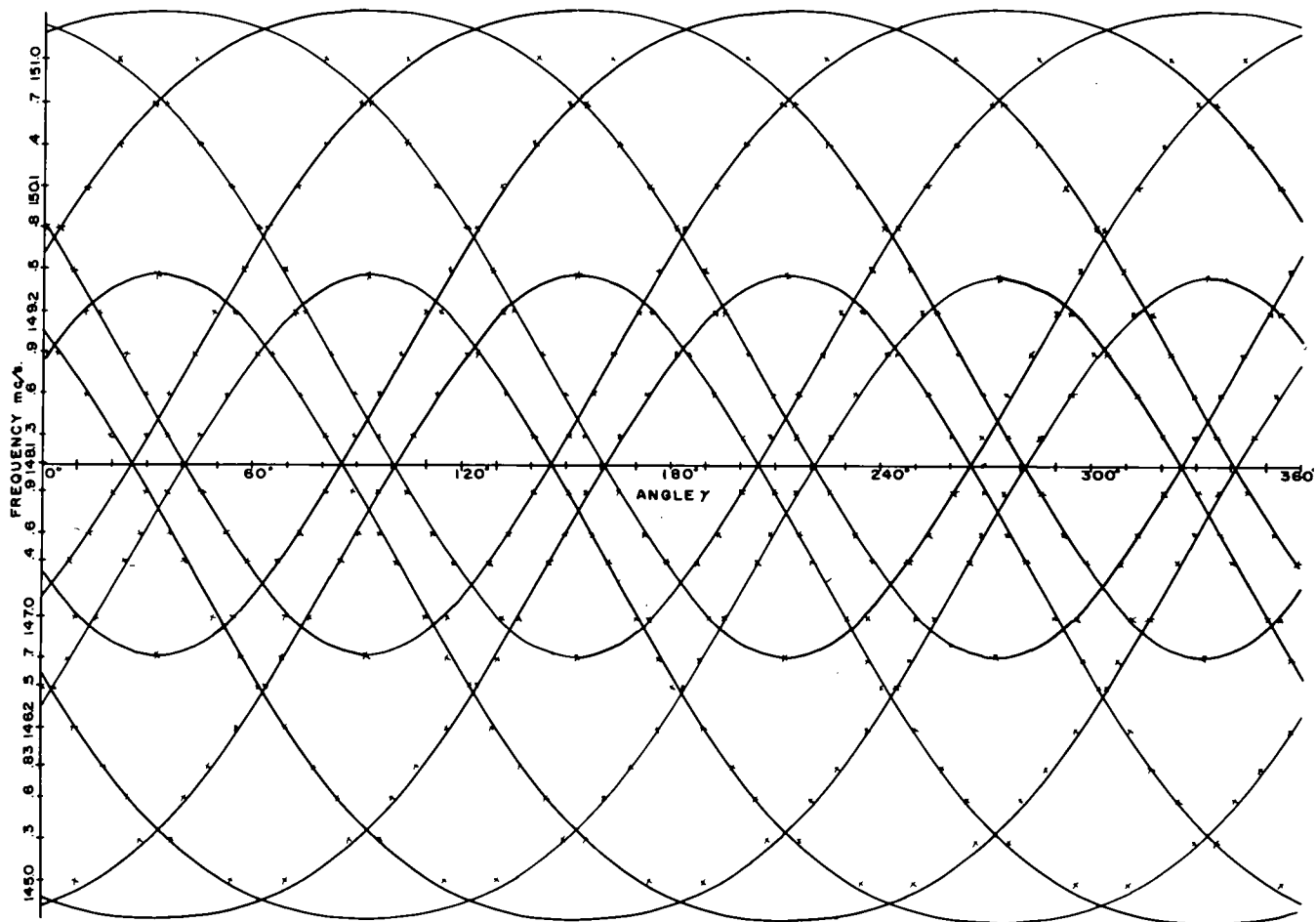


LABELLING OF THE Z-SYMMETRY AXES



A CRYSTAL WITH CUBIC STRUCTURE

FIGURE 10 to follow page 25



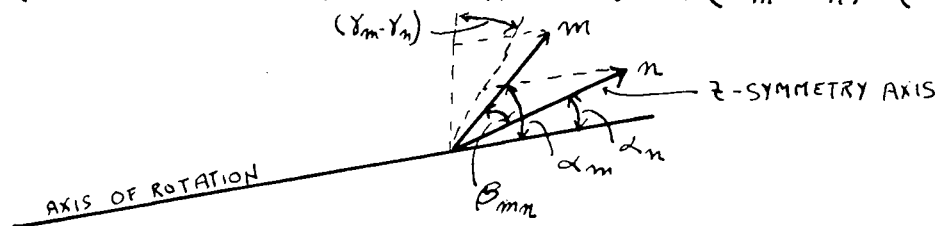
THE ZEEMAN SPLITTING OF THE NUCLEAR QUADRUPOLE RESONANCE OF Br^{81} IN A SINGLE CRYSTAL OF $\text{Zn}(\text{BrO}_{3/2}) \cdot 6\text{H}_2\text{O}$. THE (1,1,1) FACE IS PERPENDICULAR TO THE AXIS OF ROTATION. — REPRESENTS $\pm \sqrt{8} \xi \cos \gamma \pm \xi (4 - (8/3) \cos^2 \gamma)^{1/2}$
 x x REPRESENT EXPERIMENTAL RESULTS

The value of ξ was obtained by calibrating the magnetic field using the $\text{Co}(\text{BrO}_3)_2 \cdot 6\text{H}_2\text{O}$ crystal with two of the $\{111\}$ type faces perpendicular to the axis of rotation (as mentioned on page 27), and using formula (19b). This was justified because the crystal seemed to be accurately mounted and experimentally it had cubic symmetry with negligible asymmetry.

Because of the combination at times of weak signals and several sidebands some of the experimental points (Figure 10) may be in error by ± 50 kc/s., the quench frequency used. However, the plot shows that formula (30) is satisfied closely which indicates that the crystal has a cubic structure and the asymmetry parameter is negligible to a first approximation.

The angles in space β_{mn} ; $m, n = 1, 2, 3, 4$; $m \neq n$ of the z-axes were found with the aid of

$$\cos \beta_{mn} = \cos \alpha_m \cos \alpha_n + \sin \alpha_m \sin \alpha_n \cos (\gamma_m - \gamma_n) \quad (31)$$



Here $\sin \alpha$ is calculated with the aid of formula (31). Second order frequency changes in the split lines to the magnetic field are subtracted out.

Using formulae (30), (31) and (17b) Tables 1 and 2 were prepared. An estimate of the experimental accuracy was obtained from the two values of β_{24} given by each table. The two values differ by $1^\circ 24'$. All the values given fall within $70^\circ 32' \pm 47'$ where $70^\circ 32'$ is the value expected from symmetry considerations. The value of η as indicated by the angles at which the inner and outer lines coincide is estimated to be less than 0.05 since the

T A B L E 1

to follow page 26

OBSERVATIONS OF THE ZEEMAN SPECTRA OF
 $Z_n(\text{B}_r\text{O}_3)_2 \cdot 6\text{H}_2\text{O}$ AND CALCULATIONS OF THE
CRYSTAL FIELD PARAMETERS

#1 Z-symmetry axis parallel to axis of rotation

H = 1430 gauss $Z_n(\text{B}_r\text{O}_3)_2 \cdot 6\text{H}_2\text{O}$

Maximum frequency separation Dial reading γ
between inner lines

#2	2.789 mc/s	240.0 °
#3	2.748	359.1 °
#4	2.794	119.8 °

$\sin \alpha$ where α is the angle between the Z-symmetry
axis and the axis of rotation

#2	.9458
#3	.9415
#4	.9465

Angles β_{mn} between the Z-symmetry axes

$$\beta_{42} = 69^\circ 47' \quad \beta_{23} = 71^\circ 07' \quad \beta_{43} = 69^\circ 45'$$

Dial reading γ where inner and outer lines coincide

#2	292.4 °	,	187.6 °
#3	306.9 °	,	51.4 °
#4	171.8 °	,	67.8 °

Observed angles of coincidence

Calculated angles ($\eta = 0$)

#2	52.4 °	52.4 °
#3	52.3 °	52.2 °
#4	52.0 °	52.4 °

OBSERVATIONS OF THE ZEEMAN SPECTRA OF
Zn(BrO₃)₂·6H₂O AND CALCULATIONS OF THE
CRYSTAL FIELD PARAMETERS

#3 Z-symmetry axis paralalled to axis of rotation

H = 1430 gauss

Zn(BrO₃)₂·6H₂O

	Maximum frequency separation between inner lines	Dial reading δ
#1	2.704 mc/s	240.0 °
#2	2.780	359.8 °
#4	2.706	119.4 °

$\sin \alpha$ where α is the angle between the Z-symmetry axis and
the axis of rotation

#1	.9365
#2	.9450
#4	.9366

Angles β_{mn} between the Z-symmetry axes

$$\beta_{42} = 71^\circ 11' \quad \beta_{21} = 71^\circ 01' \quad \beta_{41} = 70^\circ 27'$$

Dial reading δ where inner and outer lines coincide

#1	292.0 °	,	187.9 °
#2	307.2 °	,	52.3 °
#4	171.6 °	,	67.3 °

	Observed angles of coincidence	Calculated angles ($\eta = 0$)
#1	52.1 °	51.9 °
#2	52.6 °	52.3 °
#3	52.1 °	51.9 °

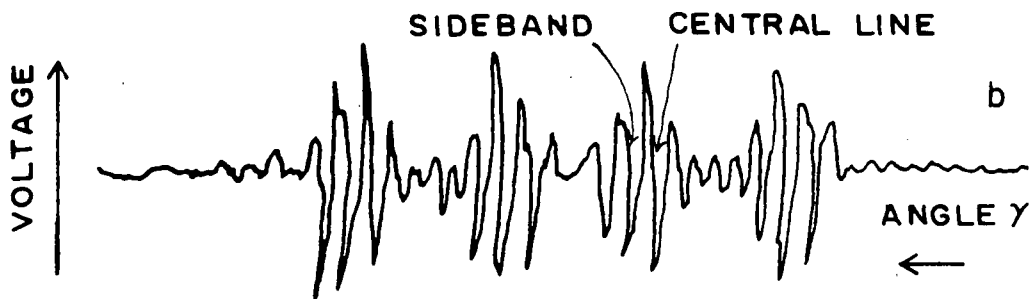
FIGURE II

refollow page 26

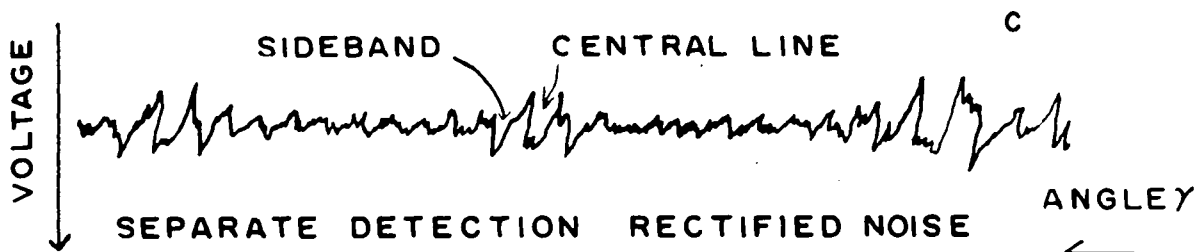
ZEEMAN SPLIT RESONANCES OF $Zn(BrO_3)_2 \cdot 6H_2O$



SELF DETECTION WITH PHASE SENSITIVE DETECTION



SEPARATE DETECTION WITH PHASE SENSITIVE DETECTION



SEPARATE DETECTION RECTIFIED NOISE

CRYSTAL MOUNTED WITH THE (111) FACE
PERPENDICULAR TO THE AXIS OF ROTATION

determinations seem to be limited by the 0.2° error in the dial reading and the line width of the split lines.

According to Groth⁵, $\text{Co}(\text{BrO}_3)_2 \cdot 6\text{H}_2\text{O}$ as well as $\text{Zn}(\text{BrO}_3)_2 \cdot 6\text{H}_2\text{O}$ has a cubic structure. A crystal of $\text{Co}(\text{BrO}_3)_2 \cdot 6\text{H}_2\text{O}$ was mounted so that $(1,1,1)$ and $(1,1,\bar{1})$ faces were parallel to the axis of rotation and the $(1,\bar{1},1)$ and $(1,\bar{1},\bar{1})$ faces each made an angle of 54.7° with the axis of rotation. Table 3 was prepared using formulae (30), (31) and (17). Table 3 gives the angles between the Z-axes of the electric field. Similar considerations of error as for $\text{Zn}(\text{BrO}_3)_2 \cdot 6\text{H}_2\text{O}$ apply except for the two Z-axes at 54.7° to the axis of rotation. Since the rate of change of frequency with angle γ was slow the lines were harder to position accurately than the others. Table 4 deals with the observation of second order effects caused by the magnetic field as given by formula (18).

The unsplit resonance frequency of $\text{Ni}(\text{BrO}_3)_2 \cdot 6\text{H}_2\text{O}$ was found to be $148.246 \pm .030$ mc/s at room temperature with a line width of about 10 kc/s. The signal to noise ratio was about one-fourth that of the unsplit resonance from $\text{Zn}(\text{BrO}_3)_2 \cdot 6\text{H}_2\text{O}$. The determination of the directions of the principal axes of the electric field gradient tensor as well as the asymmetry parameter in this salt would be of interest since, according to the "Handbook of Chemistry and Physics" this crystal has a monoclinic structure whereas, according to Groth, this crystal has a cubic structure as do the other two crystals studied here. Also, if $\text{Ni}(\text{BrO}_3)_2 \cdot 6\text{H}_2\text{O}$ is monoclinic then the information about the electric field gradient cannot be deduced from crystal symmetry.

Unfortunately the Zeeman split resonances were not observed. This is believed to be due to the weaker, broader unsplit resonance produced by this crystal compared to that of $\text{Zn}(\text{BrO}_3)_2 \cdot 6\text{H}_2\text{O}$. However, the signal to noise ratio might be improved enough to obtain fairly accurate data by increasing

OBSERVATIONS OF THE ZEEMAN SPECTRA OF
 $\text{Co}(\text{B}_2\text{O}_3)_2 \cdot 6\text{H}_2\text{O}$ AND CALCULATIONS OF THE
CRYSTAL FIELD PARAMETER

#1 and #3 Z-symmetry axes perpendicular to axis of rotation

H = 1430 gauss

$\text{Co}(\text{B}_2\text{O}_3)_2 \cdot 6\text{H}_2\text{O}$

Maximum frequency separation
 between inner lines

Dial reading γ

#1 3.296 mc/s

53.2°

#2 3.299

123.7°

$\sin \alpha$ where α is the angle between the Z-symmetry axis and
 the axis of rotation

#1 1.000

#2 1.000

Angle β_{mn} between the Z-symmetry axes

$$\beta_{13} = 70.5^\circ$$

Dial reading δ where inner and outer lines coincide

#1 358.6°

107.9°

#3 178.6°

68.9°

#2 and #4 358.2°

178.2°

Observed angles of coincidence

Calculated angles ($\eta = 0$)

#1 54.7°

54.7°

#3 54.9°

54.7°

#2 and #4 90.0°

90.0°

Assuming $\eta = 0$ and using formulae (17b) and (31) then

$$\beta_{24} = 70.5^\circ$$

$$\beta_{12} = 70.7^\circ$$

$$\beta_{14} = 70.4^\circ$$

T A B L E 4

to follow page 27

OBSERVATIONS OF SECOND ORDER EFFECTS OF
THE ZEEMAN SPLITTING OF THE NUCLEAR QUAD-
RUPOLE RESONANCE OF $\text{Co}(\text{BrO}_3)_2 \cdot 6\text{H}_2\text{O}$.

$\text{Co}(\text{BrO}_3)_2 \cdot 6\text{H}_2\text{O}$ with #1 and #3 Z-symmetry axes perpendicular
to axis of rotation

$$H = 1416 \text{ gauss} \qquad \frac{25^2}{3A} = 18 \text{ kc/s}$$

Unsplit resonance frequency 147.926 mc/s

Dial reading γ Frequency difference between
unsplit line and coincidence
of inner and outer line.

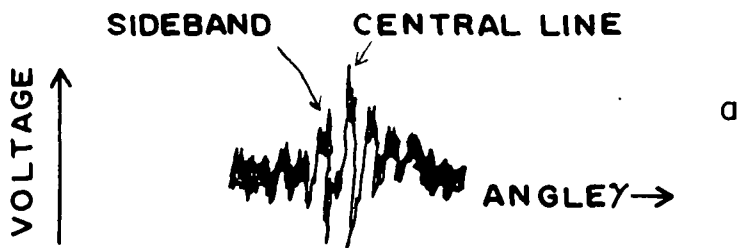
17.7 °	24 kc/s
87.8 °	23
158.6 °	23
197.4 °	21
268.0 °	22
338.5 °	22

Unsplit resonance frequency 147.930 mc/s

	γ	Observed frequency	Calculated frequency
Outer line (++)	87.8 °	150.778 mc/s	150.756 mc/s
	268.0 °	150.776	150.756
Outer line (--)	87.8 °	145.119	145.104
	268.0 °	145.120	145.104

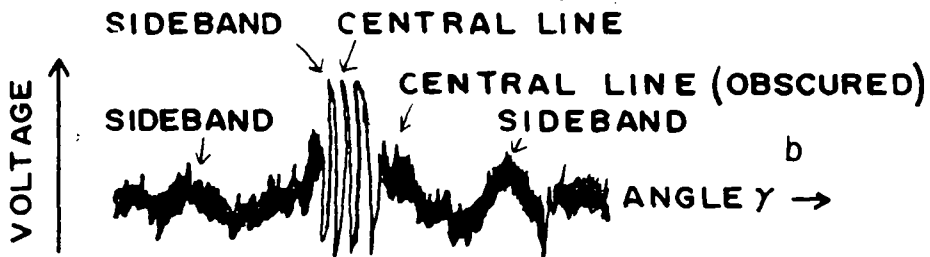
FIGURE 12 to follow page 27
 ZEEMAN SPLIT RESONANCES OF $\text{Co}(\text{BrO}_3)_2 \cdot 8\text{H}_2\text{O}$

SEPARATE DETECTION RECTIFIED NOISE



COINCIDENCE OF AN INNER AND AN OUTER LINE

CRYSTAL MOUNTED WITH THE (111) FACE
 PERPENDICULAR TO THE AXIS OF ROTATION



COINCIDENCE OF FOUR INNER AND FOUR OUTER LINES

CRYSTAL MOUNTED WITH THE (111) AND $(\bar{1}\bar{1}\bar{1})$
 FACES PARALLEL TO THE AXIS OF ROTATION

the sample size, lowering the sample temperature, and using a more homogeneous magnetic field. In conclusion the following has been achieved.

(i) A nuclear quadrupole resonance spectrometer has been built to work on narrow band operation with sufficient stability to measure the Zeeman splitting of the nuclear quadrupole resonance lines of B_r^{81} at 148 mc/s.

(ii) This instrument is sufficiently stable to detect second order effects in the Zeeman splitting of these lines but not to measure these quantitatively.

(iii) Two salts, $Zn(B_rO_3)_2 \cdot 6H_2O$ and $Co(B_rO_3)_2 \cdot 6H_2O$ have been examined. Both have been reported to be cubic in structure, although little data is given for the cobalt salt. The nuclear quadrupole resonance spectrum is consistent with a cubic crystal structure. There are 4 non-equivalent $(B_rO_3)^-$ ions per unit cell. To within the accuracy of the experiments, the principal axis of the electric field gradient at the B_r site is along the $\{1,1,1\}$ crystal axes, and the asymmetry, which for this cubic structure should be zero, is measured to be less than 0.05 in each case.

(iv) An unsuccessful attempt was made to determine the crystal field parameters in monoclinic $Ni(B_rO_3)_2 \cdot 6H_2O$. In this system these parameters are not determined by symmetry considerations. The reason for lack of success was poor signal to noise ratio for the weak, broad lines in this salt.

B I B L I O G R A P H Y

1. C. Dean, "Zeeman Splitting of Nuclear Quadrupole Resonances", *The Physical Review*, Vol.96, No.4, 1053-1059, November 15, 1954.
2. C. Dean and M. Pollak, "Suppressing Side-band Interference in Super-regenerative r.f. Spectrometers", *The Review of Scientific Instruments*, Vol.29, No.7, pp 630-632, July 1958.
3. H.G. Dehmelt, "Nuclear Quadrupole Resonance", *American Journal of Physics*, Vol.32, No.3, pp 110-120, March 1954.
4. Beverley Joan Fulton, "A Nuclear Quadrupole Resonance Spectrometer", M.A. Thesis, University of British Columbia, Vancouver, B.C., 1956.
5. P. Groth, "Chemische Krystallographie", Vol.2, pp 112, Wilhelm Engelmann, Leipzig, 1906.
6. Charles D. Hodgman, Edit. "Handbook of Chemistry and Physics" 40th Edition, Chemical Rubber Publishing Co., Cleveland, 1959.
7. Kenji Shimomura, "Structural Investigation by Means of Nuclear Quadrupole Resonance I (Determination of Crystal Symmetry)" *Journal of the Physical Society of Japan*, Vol.12, No.6, pp 652-657, June 1957.
8. S.N. Van Voorhis, Edit. "Microwave Receivers", Vol.18, M.I.T. Radiation Laboratory Series, McGraw-Hill Book Co., New York, 1948.
9. J.R. Whitehead, "Super-regenerative Receivers", Cambridge University Press, 1950.
10. Ralph W.G. Wyckoff, "Crystal Structures", Vol.II, Chap.X, text page 32, Interscience Publishers Inc., New York, 1951.